Modelling and Control of an Extruder Cooling System

Christopher Fritzon

Nils Persson

LUND UNIVERSITY

Department of Automatic Control

MSc Thesis
TFRT-6132
ISSN 0280-5316

Department of Automatic Control
Lund University
Box 118
SE-221 00 LUND
Sweden

Printed in Sweden by Tryckeriet i E-huset
Lund 2021

Abstract

The thesis aims to develop knowledge of the physics and thermodynamics behind a nonlinearity in an air cooling system for an plastic extruder machine. To accomplish this, both nonlinear and linearized models were set up in Matlab and Simulink environments based on the laws of physics and thermodynamics. Simulations were run to achieve and analyze step responses, and different PI control structures were simulated and discussed. The dynamics of the centrifugal fan were pointed out as the primary reasons for the nonlinearity. Finally, different options and alternatives, both mechanical and software based, to compensate for the nonlinearity were presented.

Due to Covid-19, it was not possible to perform any tests on real hardware which was highly desirable. Instead, the results obtained in this thesis are base solely on theoretical discussions and simulations. Aspects that potentially could have been discovered through mechanical tests are therefore not considered.

Acknowledgements

We would like to thank our academic supervisor Tore Hägglund and company supervisor Erik Ottosson for their dedication in helping us throughout this project. They have assisted us in numerous valued discussions and have given a lot of meaningful inputs that helped improve the quality of our work. A huge thank you is also directed to B&R Automation Austria employees Martin Staudecker and Johannes Senzenberger for their help on process specific matters and for providing data for model comparison and validation. Everyone involved in this thesis adhered to the Covid-19 restrictions over the course of the project, and despite the difficulties in having advanced theoretical discussions from remote the thesis is deemed successful.

Contents

List of Figures

List of Tables

List of Equations

1

Introduction

One of the major industries today and what has been for a long time is the plastic industry. Lately, the plastic production worldwide has dropped due to bans on single-use consumer plastics and plastic bags, yet 368 million tons of plastic were produced in 2019 [*Global production of plastics since 1950* 2021]. There exist many different methods on how to produce and manufacture plastic, such as injection molding, blow molding, and rotational molding. Plastic waste is recycled using a method called *extrusion*, where the recycled plastic in the form of solid pellets are being melted and reconstituted into a finished component of any desired form.

1.1 Background

B&R Industrial Automation is a company originating from Austria which was founded in 1979 and has since expanded to having offices all over the world. B&R is focusing on automation and process control technology, and is operating within many different industries – automotive, maritime and offshore, energy, and plastics to name a few.

Today, plastic processing machinery has to be more adaptable and efficient than ever to cope with different settings and demands, and due to environmental aspects a lot of plastic is being recycled. A portion of B&R's work within the plastic industry involves recycled plastics and hence controlling of plastic extruder machinery. The extrusion process itself is quite complicated, and requires both rigorous mechanical and temperature controlling to yield satisfactory results [*Automation solutions for the plastics industry* 2021].

1.1.1 The Extrusion Process

The primary function of the plastic extrusion machine is to convert solid plastic pellets into a molten plastic mass that then can be used to create products in any shape or size. There are different product categories that all rely on this machine -

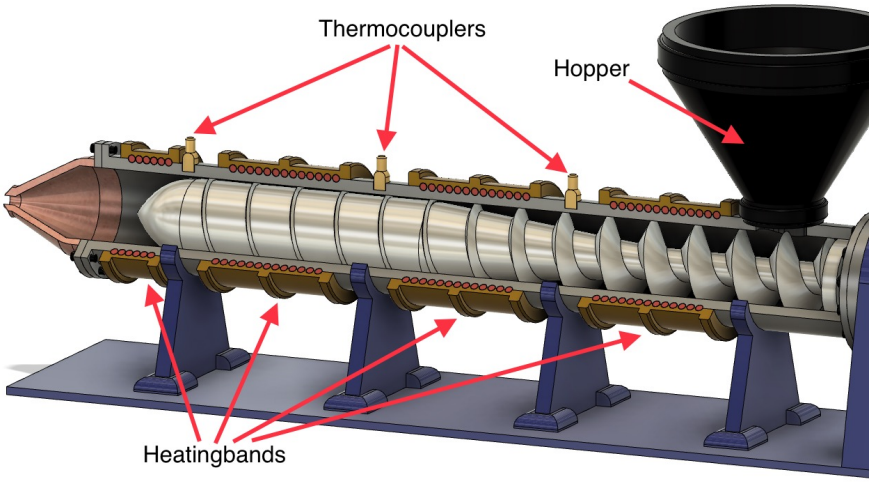

Figure 1.1: Plastic extrusion machine.

pipes, different types of extrusions, blow moldings i.e., bottles and different injection moldings to mention a few.

A plastic extrusion machine, see Figure 1.1, typically consists of a hopper that holds the plastic pellets, a barrel in which a form of screw conveyor is mounted, some ceramic heating bands, a cooling system and a couple of temperature sensors or thermocouplers. The size of the machine differs depending on the application, and typically ranges from small-scale extruders to machines in which the barrel is several meters long. A cross section of the machine with the terminology used in the thesis can be seen in Figure 1.2. The temperature sensor/theromcoupler seen in the figure is located approximately half an inch inside the barrel wall.

The barrel is divided up into zones, and in each zone heating and/or cooling is available through heating bands and a cooling system. The machines can either have air cooling or water cooling. Inside the barrel one finds the screw conveyor. The screw is usually divided up into three different zones – the *feed* zone, the *compression* zone and the *metering* zone. The channel depth of the screw, defined as the distance between the cylindrical root of the screw and the edge of the threads, varies depending on the zone, see Figure 1.3 [*A simple plastic extrusion screw* 2021].

The plastic pellets are fed gravitationally through an isolated hole in the barrel to the feed zone of the conveyor screw. The channel depth in the feed zone is constant and the deepest throughout the screw. The barrels section corresponding to the screw's feed zone is heated, thus the pellets begin to melt when in the feed zone. The screw rotates and pushes the melting pellets forwards towards the compression zone. In

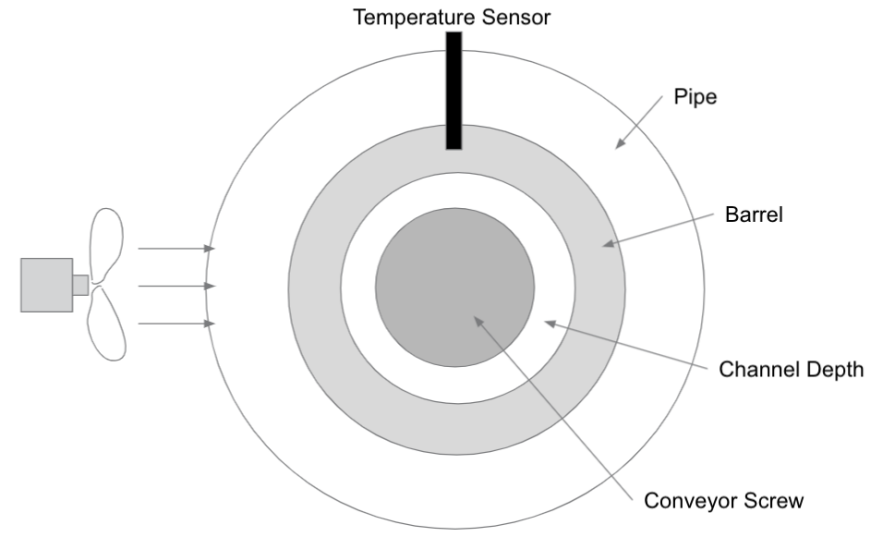

Figure 1.2: Cross section of the extruder.

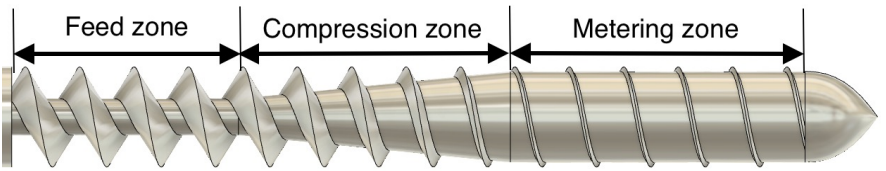

Figure 1.3: Screw conveyor.

the compression zone, more heat is applied and the channel depth is progressively becoming smaller, which forces the pellets to fuse into a molten plastic mass. As the plastic enters the metering zone, most of it is melted. In this zone, the channel depth is yet again constant however smaller then that of the feed zone. In this zone, the molten plastic is mixed to form a uniformly tempered mass. In the metering zone, the temperature of the molten plastic mass is typically above 210 $^{\circ}C$. Depending on what kind of application or item that is to be constructed, the desired temperature of the plastic when it reaches the nozzle varies between 160 $^{\circ}C$ to 300 $^{\circ}C$ which implies that the plastic mass has to be cooled.

The cooling can either be handled by air cooling or water cooling, with air cooling being less complex and it requires less components, thus it is cheaper yet less efficient. For air cooling, a centrifugal fan is powered by a three-phase electric motor.

Surrounding air is being sucked into the inlet of the fan, which then is blown out in an isolated pipe surrounding the barrel. To enhance the cooling effect, heat sinks or cooling fins are mounted in the pipe that is connected to the barrel which increases the cooling surface, see Figure 1.4. An outlet for the air to escape through after having absorbed heat from the barrel is placed on top of the pipe.

(a) Air cooling fan.

(b) Cooling fins.

Figure 1.4: Air cooling system.

1.2 Problem Formulation

A suitable temperature profile is highly important for creating the perfect plastic consistency and viscosity when exiting the nozzle. Different product specifications require different temperature profiles, however the plastic may be heated to well above the final outgoing temperature to make sure that the pellets have been fused properly. This to limit the chance of a brittle final product caused by irregularities in the plastic which in turn resides from not having created a uniformly molten plastic mass before injection or extrusion. As mentioned previously there are different heating zones, and in the case with B&R extruder systems the zones may be configured as either only heating, heating and cooling or only cooling zones.

Currently B&R have working presets for the controllers handling both the heating as well as the cooling, however especially in the cooling department there are further improvements to be made. The cooling power of the fan can be controlled by sending a PWM or PFM signal to relays connecting the three phases of the asynchronous electrical motor to mains. If relays are being used for switching instead of

semiconductors, then the PWM control signal has to be quite long due to limitations on the switching speed.

A step response for the system was performed whilst the cooling was running at 90 %. This response has then been linearly approximated and the controller tuned accordingly. Whilst running the fan at less power than the aforementioned 90 %, it was discovered that there are nonlinearities introduced somewhere in the process, see Figure 1.5. In other words the approximation is only accurate if the fan is running close to or at full power.

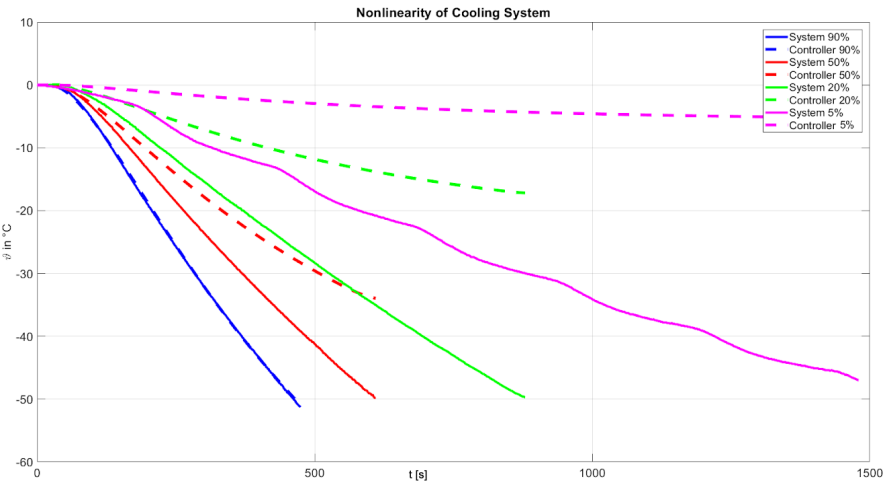

Figure 1.5: Extruder cooling nonlinearity discovered by B&R. The solid lines demonstrate the real data corresponding to a step response, while the dotted lines demonstrate a linear approximation created using the 90 % step response as a reference. The nonlinearity here becomes clear, since if the process were linear then the difference between the solid and dotted lines of the same color would be close to zero.

As B&R acquiesces a lack of knowledge of the physics behind the cooling process, the objectives of this thesis are set to

- develop knowledge of the physics behind the cooling system in general and identify the nonlinearities in particular,
- create a MATLAB/Simulink model of the system,
- improve the control strategy for the cooling.

1.3 Division of Work

The work has not been divided up between the project group members in any specific way. Instead, both have contributed with all parts and most of the work have required a lot of theoretical discussions, and as a result of that more or less all work have been performed together, remotely.

2

Physics and Modulation

No substantial literature covering the more specific subjects relating to the cooling of extruder processes were found during an initial literature analysis, thus the basis of the thesis is *Newton's law of cooling* and the first law of thermodynamics - the *law of conservation of energy* [Tipler and Mosca, 2007].

Newton's law of cooling states that *the rate of heat loss of a body is proportional to the temperature difference of the body and its surroundings*, and can be mathematically expressed as

$$\begin{aligned} Q &= hA(T(t) - T_{env}) \\ &= hA\Delta T, \end{aligned} \tag{2.1}$$

where $Q[W]$ is the rate of heat loss of the body, $h[W/(m^2K)]$ is the heat transfer coefficient, $A[m^2]$ is the boundary area between the body and its surroundings, $T(t)[K]$ is the temperature over time of the body and $T_{env}[K]$ is the temperature of the environment [Tipler and Mosca, 2007].

The law of conservation of energy states that *the total energy of an isolated system is conserved over time*. Furthermore, from the law it is clear that energy can neither be created nor destroyed but rather transforms from one form into another.

2.1 Specific Heat Capacity

The concept of specific heat was founded by Scottish scientist *Joseph Black*, who in the 18th century discovered that equal masses of different substances needed different amounts of heat to raise them through the same temperature interval [*Joseph Black (1728-1799): Discoveries* 2021]. Mathematically, the energy, q, in Joules, required to raise a body of mass m through a temperature interval ΔT is given by

$$q = mc\Delta T \tag{2.2}$$

where c is the specific heat capacity of the body [Tipler and Mosca, 2007].

2.2 Heat Convection

Convection is a thermodynamic term that describes the transfer of heat between two places from the movement of fluids. In liquids and gases, convection is typically the most dominant form of heat transfer and it comes in two distinguished forms - *free* and *forced* convection. Free convection occurs naturally and is caused by buoyancy forces as a result of density variations due to temperature differences in the fluid. Forced convection, on the other hand, occurs when an external force, such as a pump or a fan, creates currents or flows in the fluid. Mathematically, heat convection is modelled as

$$Q = h_c A(T_s - T_f), \tag{2.3}$$

where h_c is the heat transfer coefficient, A is the surface area, T_s is the surface temperature and T_f the fluid temperature.

2.3 Heat Transfer Coefficient

The *heat transfer coefficient* is the proportionality constant between the heat flux (thermal power per unit area) and the thermodynamic force that drives the flow of heat through a material. The heat transfer coefficient depends on the thickness of the material, its thermodynamic properties as well as the behaviour and properties of the surrounding environment. Consider a uniform wall with thickness s and thermal conductivity k, then the overall heat transfer coefficient, U, of the wall is given by

$$1/U = 1/h_{c,i} + s/k + 1/h_{c,o}, \tag{2.4}$$

where $h_{c,i/o}$ is the individual *convection* heat transfer coefficient of the fluid on the respective side of the wall [Tipler and Mosca, 2007].

2.4 Airflow Modulation

In this section, the fundamentals of airflow control is discussed. This can be done using different methods, with solutions ranging from physically altering the flow or to electrically regulate the speed of the motor that is powering the fan.

2.4.1 Fan speed modulation

Changing categories of manipulation methods, it is possible to implement methods for regulating the speed at which the motor shaft rotates which in turn generates the airflow. There are two paths for doing this - the first is to change the frequency with which the motor is supplied and thus create a constant rotational speed and constant airflow. The second alternative is to regulate the airflow average over time. This average value can be achieved by switching on and off the motor over time. This will result in the fan blowing at full speed during some time intervals and being completely still at other times.

This average can be created using either a *Pulse Width Modulation (PWM)* controller or a *Pulse Frequency Modulation (PFM)* controller. Theoretically both of these modulation methods could then make the fan output an average airflow of choice between 0-100 % of maximum airflow. In practice, however, this is problematic because of the ramp up and ramp down behaviour of the fan.

2.4.2 Frequency Modulation

The most advanced method of them all is to regulate the frequency of the alternating current supplying the motor. When directly connected to the grid the frequency is standardized to be 50Hz, but it is possible to change this using power electronics by firstly rectifying the alternating current and then adding a large smoothing capacitor. The output from this circuit is basically direct current with no oscillations. However, the motor cannot run on this voltage so the voltage has to be transformed back into alternating current. This is done using H-bridges which basically are transistors connected in such a way that the positive and negative voltages of the alternating current can be recreated. By switching these transistors on and off in a synchronised and well timed order the 3 phase alternating current can be recreated with any frequency. This is very efficient (usually 98-99% efficiency), but also probably the most expensive method.

2.4.3 Pulse Width Modulation

A *Pulse Width Modulation (PWM)* controller works by switching on and off the voltage during a set *period time*, t_{pwm}. The period time is chosen depending on the system dynamics and the length of a pulse within the period time will determine the average power output of that cycle. The *duty cycle*, D, of the PWM signal is defined as the percentage of the period time in which the signal is high, i.e.,

$$D = 100\frac{PW}{t_{pwm}}, \tag{2.5}$$

where $PW \leq t_{pwm}$ is the pulse width (high signal). For the sake of clarity, Figure 2.1 shows a PWM signal with 1 s period time and 50 % duty cycle and Figure 2.2

shows multiple PWM signals with duty cycles from 10 % to 100 %. The frequency at which the cycles are run depends on the system, and should be reasonable in comparison to the time constants of the dynamics of the system.

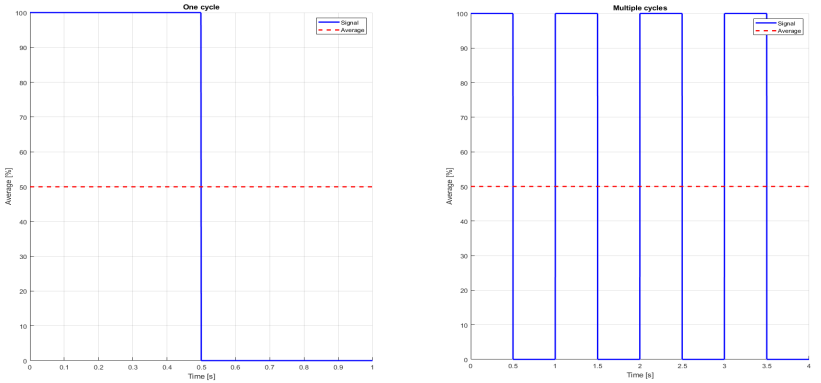

(a) 50 % duty cycle PWM signal over a single period.

(b) Multiple periods with 50 % duty cycle.

Figure 2.1: PWM signal with 1 s period time and 50 % duty cycle.

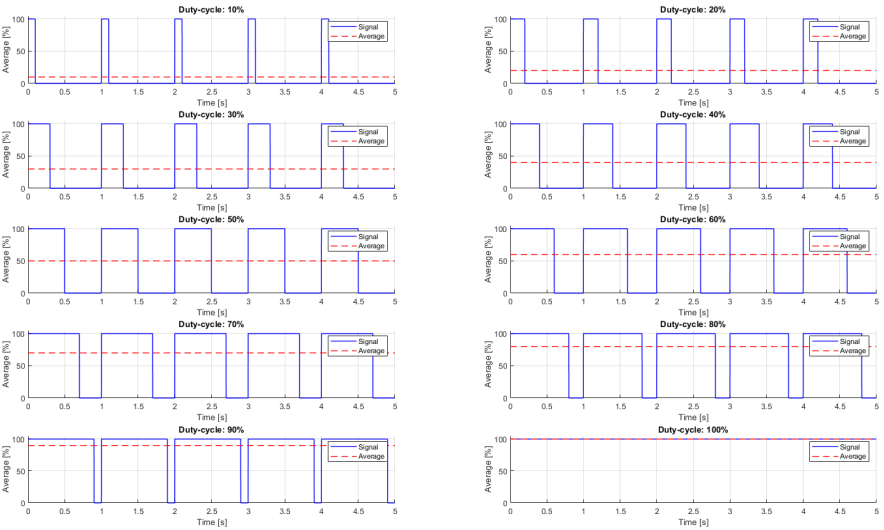

Figure 2.2: Multiple PWM signals with duty cycles ranging from 10 % to 100 %.

2.4.4 Pulse Frequency Modulation

A *Pulse Frequency Modulation (PFM)* controller is responsible for creating an analog-like signal by using only two logical levels (fully on or fully off), similar to that of a PWM controller. However, it does this by pulsating the high logic level for a fixed length of time and instead the frequency at which this pulse is sent varies. The pause time between two pulses is defined, and its minimal value is given. This creates a "pulse train" with each pulse being the same length but being sent at different times to create an overall average lower than the original "fully on" logical level. The goal is quite similar to the ones of a PWM controller.

The main difference between a PWM and PFM signal, see Figure 2.3, is that for a PWM the pulse width is varied but the frequency of the pulses is constant. For the PFM, the pulse width is fixed and the frequency varies.

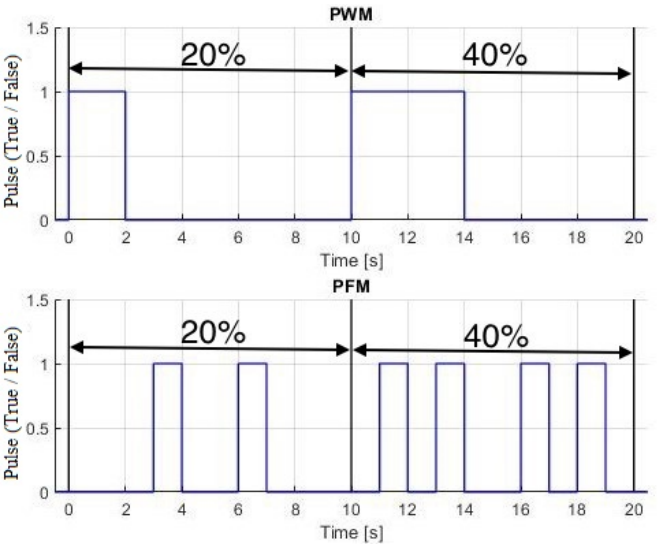

Figure 2.3: A typical PFM signal and how it differs from a PWM signal.

3

Modelling

In this chapter, models will be derived in order to mathematically and physically describe the energy transfer dynamics of the cooling system in the extrusion process. Initially, a basic model based on the conservation of energy is presented. In the model, all energy transfers within the system are expressed in terms of parameters such as temperature, mass and material-specific heat capacities. This model is then further developed, taking into account ambient losses in the second version and process disturbances in the third. Continuing, as a main objective of the thesis is to identify nonlinearities, the ramp-up and ramp-down behaviour of the centrifugal fan is discussed and modelled.

3.1 Basic Model

The cooling system of the extrusion process is modelled as two mass volumes, V_p and V_b, and an airflow $\dot{m}$, see Figure 3.1. The volume inside the pipe that surrounds the barrel is denoted V_p, and the air that fills V_p has a corresponding temperature T_p, mass m_p and specific heat capacity c_p. Similarly, V_b is said to be the volume of the barrel wall which in turn has a temperature T_b, mass m_b and specific heat capacity c_b. The input to the system is a control signal u to the motor driving the centrifugal fan, and its objective is to control the airflow $\dot{m}$. The measurable barrel temperature T_b is the output of the system.

Following from the system in Figure 3.1, the dynamics of the system are derived as

$$\begin{aligned} m_p c_p \dot{T}_p &= A\alpha(T_b - T_p) + \dot{m}c_{amb}(T_{amb} - T_p) \\ m_b c_b \dot{T}_b &= A\alpha(T_p - T_b), \end{aligned} \tag{3.1}$$

following the conservation of energy and Equations 2.1-2.4, where α is the heat transfer coefficient between the barrel and the air in the pipe, A is the surface area

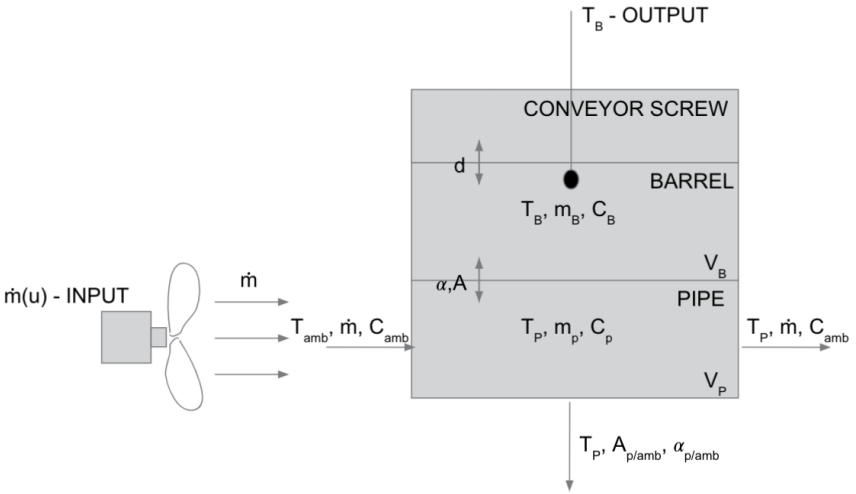

Figure 3.1: Model of the cooling process.

between the barrel and the pipe, T_{amb} is the ambient temperature in the room in which the extruder machine is located and c_{amb} denotes the specific heat capacity of the ambient air.

3.2 Model with Ambient Losses

The basic model describes a system which is completely separated from the surrounding environment in terms of thermodynamics and energy transfers. In other words, it considers the system to be perfectly isolated from the ambient air. In reality, this would not be the case as there would be energy leakage to the surroundings. In order to take care of this, a new term L_k has to be added to the dynamics which describes the ambient energy losses. It is assumed that the pipe is surrounding the entire barrel in the cooling zone, which means that the ambient losses would only occur in the V_{pipe} mass volume. The extended dynamics are then given by

$$\begin{aligned} m_p c_a \dot{T}_p &= A\alpha(T_b - T_p) + \dot{m}c_{amb}(T_{amb} - T_p) + L_k \\ m_b c_b \dot{T}_b &= A\alpha(T_p - T_b), \end{aligned} \tag{3.2}$$

where the ambient losses L_k are given by

$$L_k = A_{p/amb}\alpha_{p/amb}(T_{amb} - T_p). \tag{3.3}$$

In this case, $A_{p/amb}$ denotes the surface area between the pipe and the surrounding air with its corresponding heat transfer coefficient $\alpha_{p/amb}$.

3.3 Model with Process Disturbances

At this stage, the model only describes the system when it is empty and there is no flow of molten plastic inside the barrel. The characteristics of the molten plastic are unknown, thus it is reasonable to treat the plastic as a process disturbance. When B&R previously have tuned the extruder systems, the systems have been empty, i.e., there had been no plastic in any form located within the system. The reason for this was to simplify and speed up the cleaning process that would come as a result of an ill-tuned system. When tuning the system, the control objective is to control the barrel temperature, instead of controlling the temperature of the plastic, to a given setpoint.

After the tuning process is completed and the system is started, the plastic will fill the system as previously described and thus, naturally, the energy brought to the system by the molten plastic can be seen as a disturbance. The energy that this disturbance, d, brings to the system on average is given by

$$d = A_{innerBarrel}\alpha_{b/plastic}(T_{plastic,avg} - T_b), \tag{3.4}$$

where $A_{innerBarrel}$ is the inner area of the barrel cylinder, $\alpha_{b/plastic}$ denotes the heat transfer coefficient between the plastic and the barrel and $T_{plastic,avg}$ is the average temperature of the plastic throughout the cooling zone.

The plastic that enters the system, where *enters the system* refers to the cooling zone and not the hopper, is assumed to be 210° C at all times. Similarly, the plastic that leaves the system is assumed to have the same or a slightly higher temperature than the barrel setpoint temperature. This means that the average plastic temperature, assuming a linear behaviour between entering and leaving the system, is given by

$$T_{plastic,avg} = \frac{210 + T_{b,setpoint}}{2}. \tag{3.5}$$

The fundamentals of the process disturbance is that it brings energy to the system, which means that it should increase the temperature of the barrel. The dynamics of the disturbance from Equation 3.4 in combination with the average plastic temperature from Equation 3.5 implies that if the barrel temperature is higher than that of the average plastic temperature, then the process disturbance would actually help

cool the barrel instead. This occurs for high barrel temperatures during the start up of the machine, and is of course a cause of error in the model. To cope with it, logics is implemented in the Matlab model that modifies the dynamics such that $d \geq 0$ for all temperatures T_b.

One would think that it would be better to create a more suitable model of the temperature change in the plastic as a function of time and its mass flow in the barrel, instead of only using the average temperature. However, such a model would have large uncertainties which would add unnecessary complexity to the system.

The complete dynamics of the system is given by

$$\begin{aligned} m_p c_{amb} \dot{T}_p &= A\alpha(T_b - T_p) + \dot{m} c_{amb}(T_{amb} - T_p) + A_{p/amb}\alpha_{p/amb}(T_{amb} - T_p) \\ m_b c_b \dot{T}_b &= A\alpha(T_p - T_b) + A_{innerBarrel}\alpha_{b/plastic}(T_{plastic,avg} - T_b). \end{aligned} \tag{3.6}$$

3.3.1 Dimensions

The size of a plastic extruder may vary a lot with barrels ranging from small ones less than a meter long, to cases where the barrel is several meters long, which makes it difficult to generalize the dimensions to cover all applications. Hence, in this thesis, a fixed set of parameters defines the dimensions of the system where the values of said parameters are approximated. No data is available on size of an average system, thus the dimensions are given reasonable values depending on evaluation of given pictures in Figure 1.4 and discussions with the B&R supervisors. To be able to compare and reason about different versions of simulation results through the course of the thesis, it was deemed necessary to fix a certain amount of parameters early on.

Continuing, the total length of the barrel need not be specified for this thesis but rather the length of the cooling zone of the barrel. The barrel is of circular shape and consists of different layers of material and sections. The barrel itself consists of a 2-3 cm thick wall made of steel. Inside the barrel wall, the depth of the channel (in which the molten plastic is conveyed) between the screw and the inner walls of the barrel is approximated to 1 cm. The remaining distance between the center of the barrel and the beginning of the channel depth is defined as the screw, and totals at around 14 cm. Thus, the inner wall of the barrel starts at a radius of 15 cm from the center point with a thickness of 2-3 cm as mentioned. Surrounding the barrel are the ceramic heating bands as well as the pipe into which the centrifugal fan blows, see Figure 1.4. The pipe is around 30 cm in radius, which implies a 13 cm gap between the outer wall of the barrel and the pipe for the cooling air to flow through. These dimensions and the matching terminology for each part can be seen in Figure 3.2.

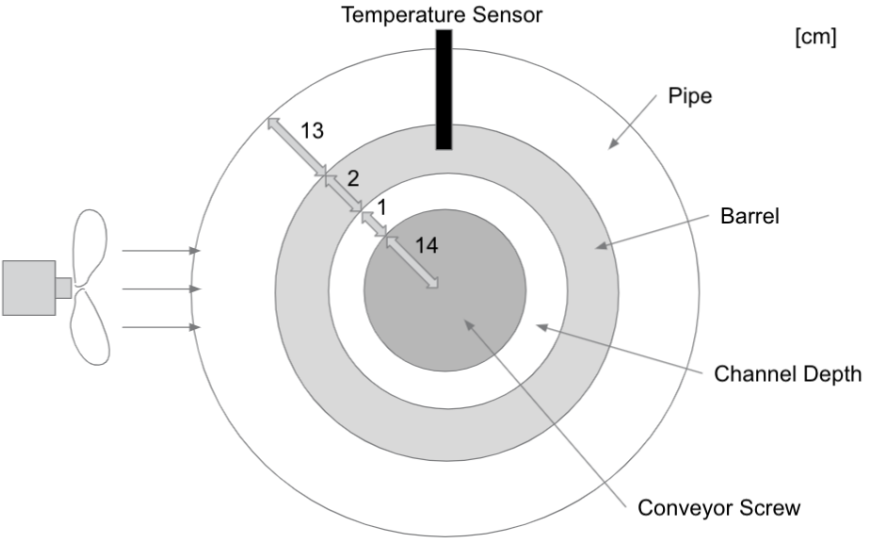

Figure 3.2: Cross section of the extruder with dimensions.

3.4 Centrifugal Fan

The centrifugal fan that is used in the cooling system is seen in Figure 1.4. A data sheet for the fan was available throughout the course of the thesis and it can be seen in Appendix A. However the information stated in it was not sufficient to build an accurate mathematical model of the delivered airflow.

Euler's Turbomachinery Equations are a set of Equations that can be used to determine and predict the effects of changing the geometry of the fan and its rotor blades [*Pump Theory - Euler's Turbomachine Equations* 2021]. The same set of Equations can be used to calculate the shaft torque, power consumption and delivered airflow given that the mentioned geometry, in addition to other parameters such as input voltage and frequency, is known. However, in this case no information about the geometry of the rotor blades nor their dimensions were given, and if these parameters were to be assumed and approximated then large errors could be introduced. Instead, the behaviour of the centrifugal fan was modelled as empiric profiles as both the ramp up and the ramp down time of the fan was known. The empiric profiles build on mass moment of inertia, I,

$$I = \frac{L}{\omega}, \tag{3.7}$$

where L is the angular momentum and ω is the angular velocity.

The delivered airflow of the centrifugal fan is directly proportional to the rotational speed of the motor that powers it [*Fan Performance and Fan Laws* 2021].

3.4.1 Ramp Up

Ideally, the fan would reach a state where maximum airflow is delivered instantly when switched on, however given the laws of physics that is not happening. Previous experiments from B&R had shown that the fan, when switched on, ramps up to full speed which produces maximum airflow in 0.5 s. After extensive discussions and logical reasoning, the ramp up behaviour of the centrifugal fan is thus modelled as in Figure 3.3. Initially, the the delivered airflow starts off exponentially and upon being close reaching its maximum value, the exponential behaviour flattens out and the airflow becomes saturated at its maximum value at around 0.5 s after being switched on.

3.4.2 Ramp Down

In similarity to the ramp up case, the required time for the centrifugal fan to come to a complete stop when it is operating full speed was determined and set at around 30 s through an experiment which B&R conducted. When the fan is shut off at maximum speed, the delivered airflow is expected to decrease exponentially as can be seen in Figure 3.3. In other words, when first shutting off the fan its speed is reduced fastest due to high air resistance and friction, but as its speed has ramped down further the resistance becomes smaller and the rate at which the speed is reduced follows.

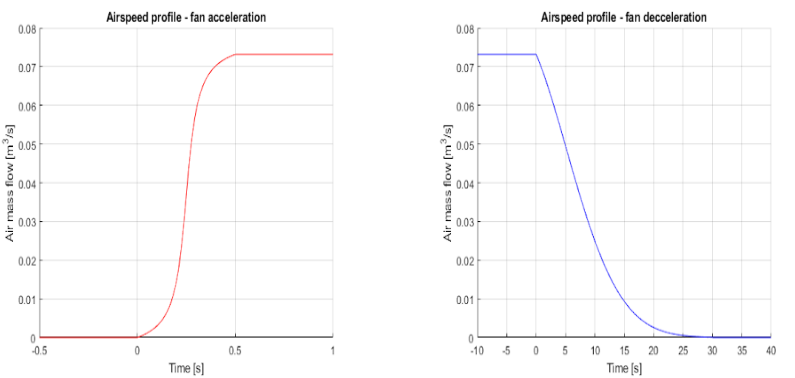

(a) Ramp up.

(b) Ramp down.

Figure 3.3: Empiric profiles of the centrifugal fan behaviour during ramp up and ramp down.

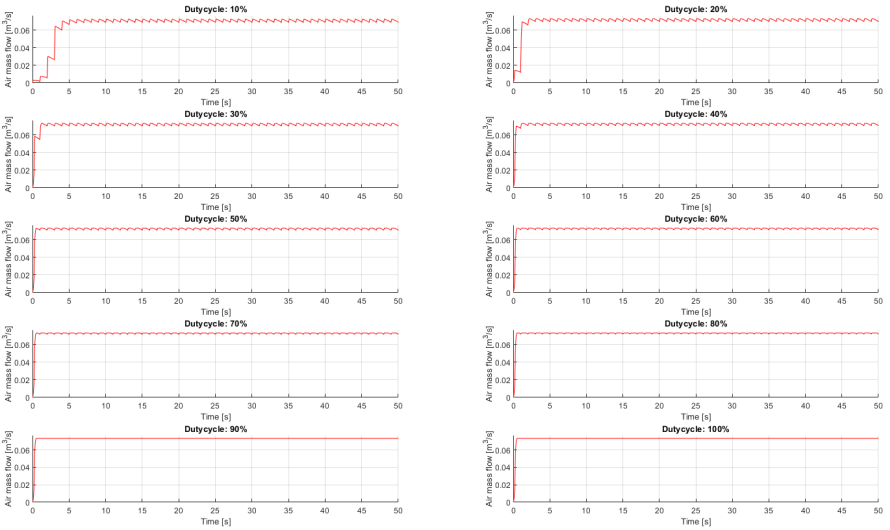

Figure 3.4: Airflow generated with duty cycles ranging from 10 % to 100 % using a PWM period time of 1 s.

3.5 Airflow model

As mentioned earlier, the dynamics of the centrifugal fan range in the time scale of 0.5 s to 30 s for ramp up and ramp down, respectively. When choosing a period time for the PWM signal, the time constants of the system must be taken into consideration. Having a period time of 1 s would make little sense since it takes around 30 s for the fan to stop when it is switched off. Ideally, the behaviour of the fan involves low-pass characteristics so that the general airflow is proportional to the duty cycle. However, since this is not physically possible with the available fan, the second best thing is if the delivered airflow follows that of the PWM signal as closely as possible. Figure 3.4 shows the airflow as a function of the PWM duty cycle, and clearly the airflow does not even come close to resembling a PWM signal. If the average airflow as a function of the desired duty cycle is calculated, then with a 1 s period time, one can see in Figure 3.5 that there is little to no controllability of the airflow - even with a duty cycle of 10 %, the delivered airflow is still close to 100 %. The maximum airflow that the fan is capable of delivering is 0.0732 m^3/s, see the datasheet in Appendix A.

If, instead of using 1 s, one chooses a period time of 10 s then the corresponding instantaneous and average airflow functions are seen in Figures 3.6 and 3.7. Here, one may visually start to see a PWM behaviour in the instantaneous airflow. In the average airflow graph, it is still clear that using a 10 s period time results in a lack of controllability.

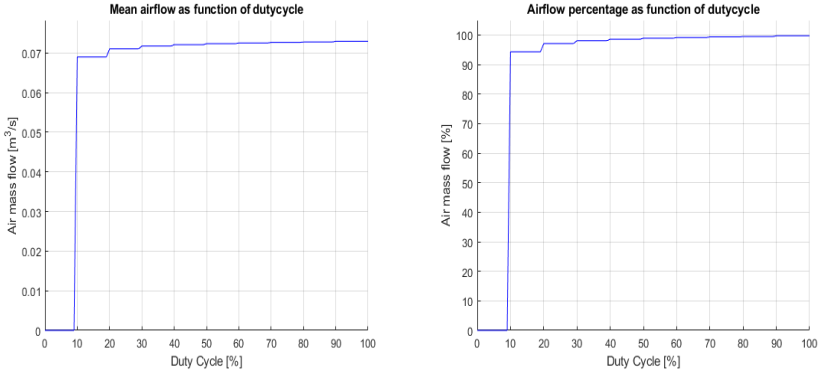

(a) Air flow.

(b) Relative air flow.

Figure 3.5: Correlation between airflow and duty cycle percentage using a cycle period time of 1 s.

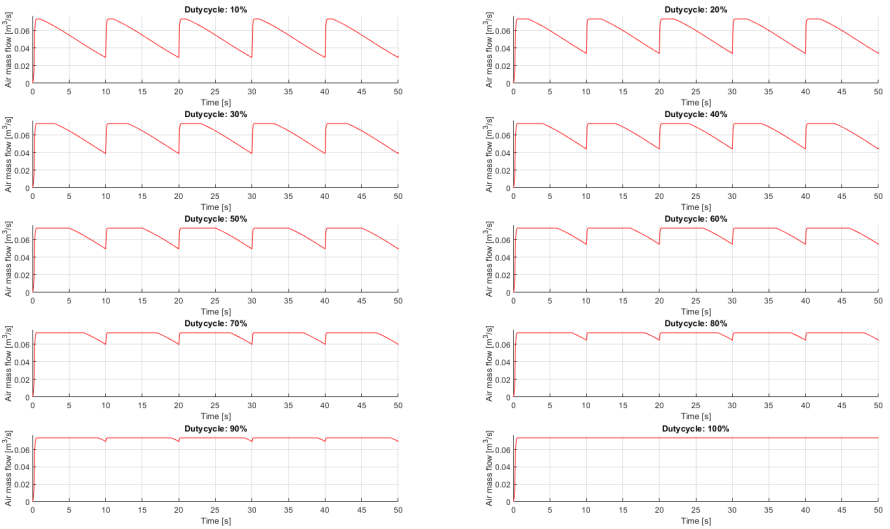

Figure 3.6: Airflow generated with duty cycles ranging from 10 % to 100 % using a PWM period time of 10 s.

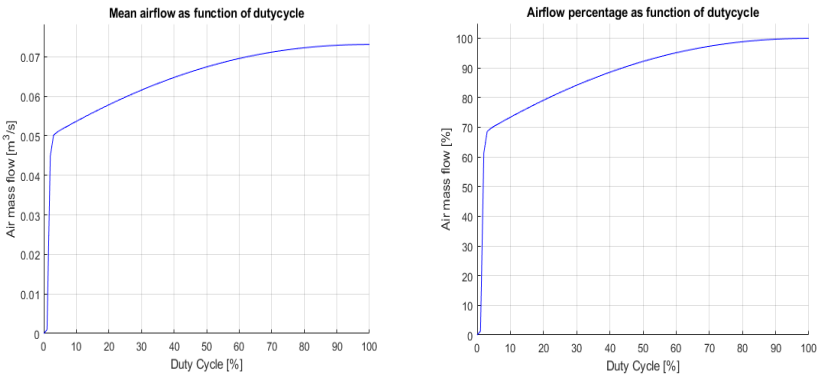

(a) Air flow.

(b) Relative air flow.

Figure 3.7: Correlation between airflow and duty cycle percentage using a cycle period time of 10 s.

When increasing the period time further to 60 s, the behaviour starts to change substantially. Now one can see that the instantaneous airflow reaches 0 for low duty cycles, which means that now the fan is actually standing still and thus no airflow is delivered. The fact that the fan may be switched off and brought to standstill all within the time of a period has a great effect on the airflow's controllability, see Figures 3.8 and 3.9.

By now, it is clear that the period time has a great impact on the controllability of the airflow that the fan delivers. Thus far, the airflow has become more controllable for higher period times. This is due to the fact that the ramp down becomes smaller in relation to the cycle time when the period is increased. Naturally one then expects the best possible results when the period time keeps increasing. However, by studying the corresponding airflow graphs when using a 100 s period time, see Figures 3.10 and 3.11, it can be seen that the controllability starts to saturate which implies that an upper bound exists for the period time.

The difference between a 60 s and a 100 s period time is not that big. Also, which will be discussed at a later stage, increasing the period time brings oscillations into play when looking at the barrel temperature over time. To summarize this section about the airflow modelling, it can be noted that the period time has a great effect on the controllability of the airflow. Furthermore, there is a trade off between airflow controllability and system oscillations which need to be considered when choosing a period time for the PWM signal. A fast period time would imply a loss of accuracy as the output airflow would be more or less constant and close to maximum due to the fan's inertia, while a longer period time results in good accuracy but could bring oscillations into play.

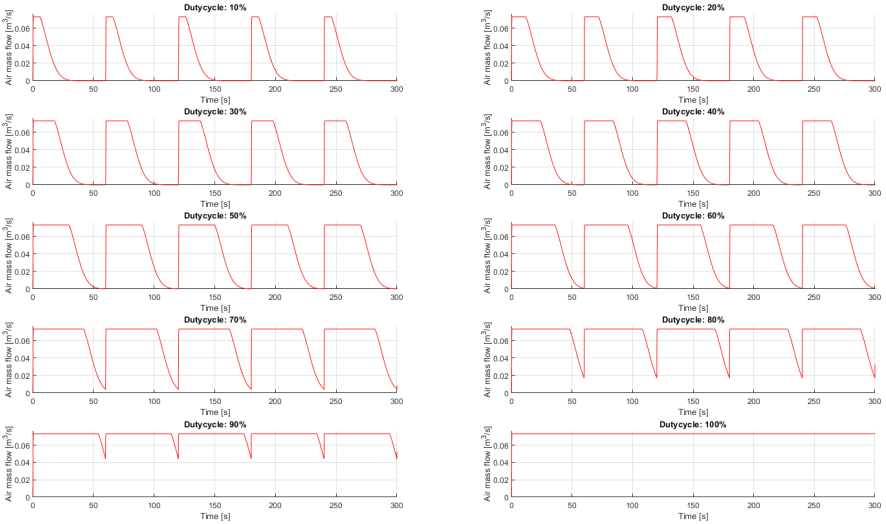

Figure 3.8: Airflow generated with duty cycles ranging from 10 % to 100 % using a PWM period time of 60 s.

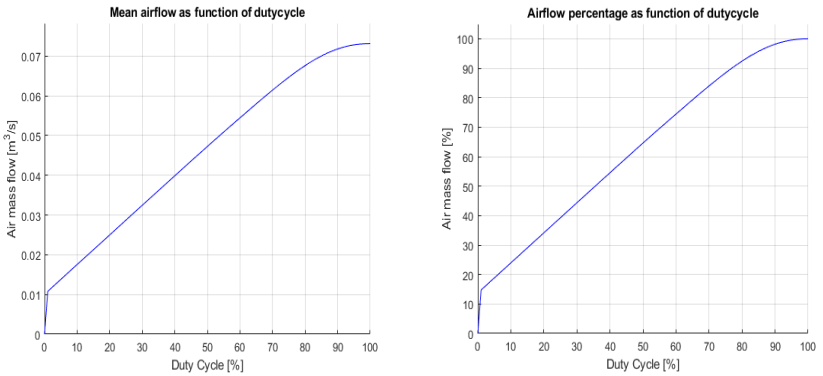

(a) Air flow.

(b) Relative air flow.

Figure 3.9: Correlation between airflow and duty cycle percentage. Using a cycle period time of 60 s.

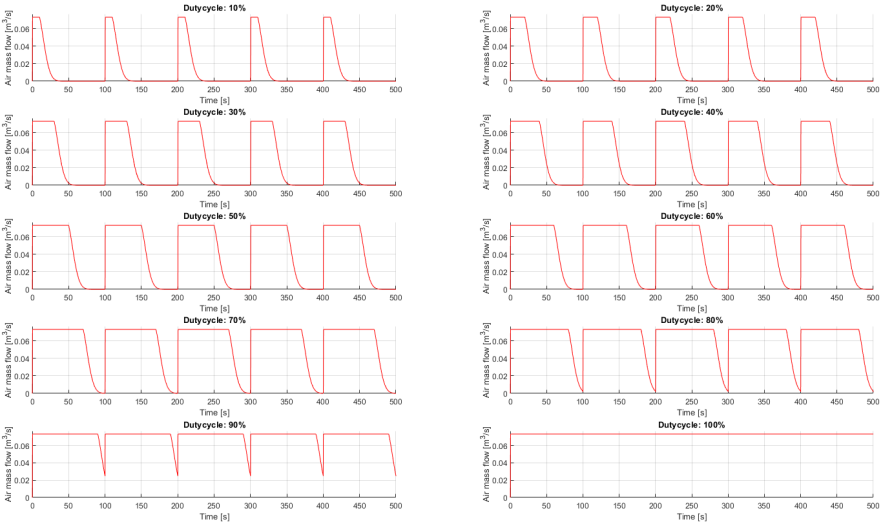

Figure 3.10: Airflow generated with duty cycles ranging from 10 % to 100 % using a PWM period time of 100 s.

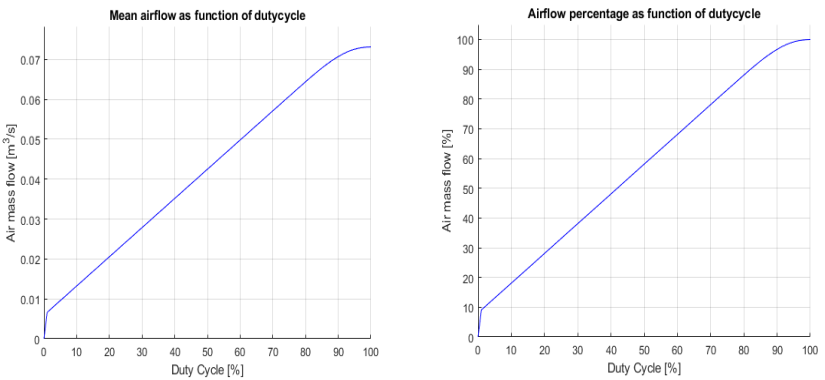

(a) Air flow.

(b) Relative air flow.

Figure 3.11: Correlation between airflow and duty cycle percentage. Using a cycle period time of 100 s.

3.6 Heat Transfer Coefficient Model

To be able to accurately calculate and model the barrel temperature, an important factor is the overall heat transfer coefficient of the system. This coefficient is determined through Equation 2.4, and an overview of the system in this regard is available in Figure 3.12. As the heat transfer coefficient depends on the behaviour of the fluids on both sides of the barrel, as well as the material properties of the barrel, it is crucial to model the heat transfer coefficient as a function of the output airflow of the centrifugal fan.

In order to model the heat transfer coefficient, it is necessary to divide the system up into different cases to cover all combinations of free and forced convection of the fluids. The inside of the barrel is considered $zone_b$, inside the pipe is considered as $zone_p$ and the ambient air is considered $zone_{amb}$, see Figure 3.12. The combinations then become,

- free convection in $zone_b$, free convection in $zone_p$ & free convection in $zone_{amb}$
- free convection in $zone_b$, forced convection in $zone_p$ & free convection in $zone_{amb}$
- forced convection in $zone_b$, free convection in $zone_p$ & free convection in $zone_{amb}$
- forced convection in $zone_b$, forced convection in $zone_p$ & free convection in $zone_{amb}$.

The combinations and what they mean in relation to the activity of the centrifugal fan and the process disturbance is summarized in Table 3.1.

Table 3.1: The different combinations of free and forced convection in the zones in regards to the centrifugal fan actions and process disturbance. There is always free convection in $zone_{amb}$.

$zone_b$	$zone_p$	$zone_{amb}$	Plastic present	Centrifugal fan
Free	Free	Free	No	Off
Free	Forced	Free	No	On
Forced	Free	Free	Yes	Off
Forced	Forced	Free	Yes	On

The values of the convective heat transfer coefficients, $h_{c,i/o}$, depend on whether the convection is free or forced, and if it is forced then the magnitude of the force comes into play. In $zone_b$, i.e., inside the barrel, there is either air or plastic. In the event of air, the convection is free and the value of $h_{c,i}$ is set to $2.5 - 25$ $[\frac{W}{m^2K}]$ [*Convection Heat Transfer Coefficient* 2021]. In the case of forced convection in the barrel, molten plastic is present and is being forced forward by the screw conveyor. As the exact thermodynamic properties of the molten plastic are unknown, the convection heat transfer coefficient has to be estimated in this case.

A moderate flow of water in a pipe has a convective heat transfer coefficient of 3000 $[\frac{W}{m^2K}]$ [*Convective Heat Transfer Coefficients Table* 2021]. Now, the flow in the barrel caused by the screw conveyor is hardly described as moderate but rather low instead, thus a low flow of water is estimated to yield a convective heat transfer coefficient of 1000 $[\frac{W}{m^2K}]$. Plastic, polypropylene in this case, typically has a specific heat capacity of $1700 - 1900$ $[\frac{J}{kgK}]$, whereas the corresponding property of water is 4200 $[\frac{J}{kgK}]$. Hence, it requires less energy to heat a unit mass of plastic compared to water. As a result of this observation, the convective heat transfer coefficient for a low flow of plastic is estimated as 1900/4200 times the convective heat transfer coefficient for a low flow of water, or about 450 $[\frac{W}{m^2K}]$.

Continuing, the convection of air in $zone_p$ is free when the centrifugal fan is off and forced when it is on. The free convection of $zone_p$ is set equal to that of the free convection in $zone_b$, but the forced convection has to be modeled as a function of the airflow. As proposed by [Bourne-Webb et al., 2016], a linear relationship between the forced convection coefficient and the airflow velocity, v, is sufficiently accurate for $v \leq 5$ $[m/s]$. However, for simplicity, this model assumes a linear dependency between the convection constant and the airflow for all velocities. For air the forced convection heat transfer coefficient ranges between $10 - 500$ $[\frac{W}{m^2K}]$, but as the maximum airflow velocity that the centrifugal fan is capable of delivering is shy of 20 m/s, the forced convection coefficient is estimated to be bound by the free convection and 250 $[\frac{W}{m^2K}]$.

In $zone_{amb}$, the convection of air is free and its heat transfer coefficient value is the same as that from the other zones.

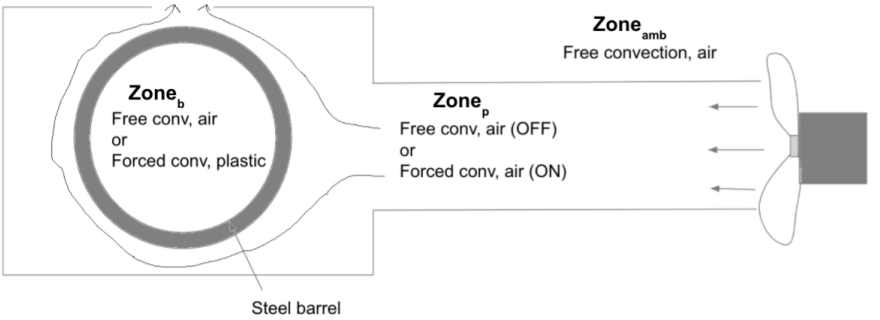

Figure 3.12: View of the centrifugal fan and the barrel with $zone_b$, $zone_p$ and $zone_{amb}$ denoting the inside and outside of the barrel and pipe, respectively.

3.7 Linearization of Nonlinear System & Transfer Functions

Amongst the initial data presented by B&R, see Table 3.2, a couple of second-order linear transfer functions on the form $H(s) = \frac{K}{(sT_1+1)(sT_2+1)}e^{-T_3 s}$ that describes a similar system can be found. This similar system has unknown physical dimensions that may differ from the system presented in this thesis. However, it was requested to obtain transfer functions of the process during this thesis as a method of verifying the process dynamics compared to the data presented by B&R. To achieve this, the nonlinear dynamics first have to be linearized and then transformed into transfer functions.

Table 3.2: Transfer functions of a linear system similar to the thesis process, based on least squares approximations. Provided by B&R.

Duty Cycle	Transfer Function
100 %	$\frac{1.41}{(51s+1)(635s+1)}e^{-15s}$
90 %	$\frac{1.14}{(70s+1)(550s+1)}e^{-20s}$
50 %	$\frac{2.5}{(61s+1)(1030s+1)}e^{-25s}$
20 %	$\frac{7.5}{(61s+1)(2000s+1)}e^{-25s}$
5 %	$\frac{22.1}{(61s+1)(2500s+1)}e^{-30s}$

In order to linearize the dynamics from Equation 3.6, it is convenient to rewrite the system on state-space form,

$$\begin{aligned} \dot{x} &= Ax + Bu \\ y &= Cx + Du. \end{aligned} \tag{3.8}$$

where x is the state vector and u is the control variable. Thus, a state vector $(x_1, x_2) = (T_p, T_b)$ is introduced, and the dynamics are rewritten as

$$\begin{aligned} \dot{x}_1 &= \frac{1}{m_p c_a}(A\alpha(x_2 - x_1) + \dot{m}(u)c_{amb}(T_{ambient} - x_1) + A_{p/amb}\alpha_{p/amb}(T_{ambient} - x_1)) = f_1 \\ \dot{x}_2 &= \frac{1}{m_b c_b}(A\alpha(x_1 - x_2) + A_{innerBarrel}\alpha_{b/plastic}(T_{plastic,avg} - x_2)) = f_2. \end{aligned} \tag{3.9}$$

The state-space matrices are obtained from the dynamics in Equation 3.6, and are

given by

$$
\begin{aligned}
A &= \begin{bmatrix} \frac{\partial f_1}{\partial x_1} & \frac{\partial f_1}{\partial x_2} \\ \frac{\partial f_2}{\partial x_2} & \frac{\partial f_2}{\partial x_2} \end{bmatrix}_{|\left[x_1, x_2, \dot{m}(u)\right] = \left[x_{10}, x_{20}, \dot{m}(u_0)\right]}, \\
B &= \begin{bmatrix} \frac{\partial f_1}{\partial u} \\ \frac{\partial f_2}{\partial u} \end{bmatrix}_{|\left[x_1, x_2, \dot{m}(u)\right] = \left[x_{10}, x_{20}, \dot{m}(u_0)\right]}, \\
C &= \begin{bmatrix} 0 & 1 \end{bmatrix}, \\
D &= 0,
\end{aligned} \tag{3.10}
$$

where $\left[x_{10}, x_{20}, \dot{m}(u_0)\right]$ is the operating point of the system. The final stage of the transfer function conversion process is to define the transfer function as $H(s) = \frac{Y(s)}{U(s)}$, and to convert the linearized dynamics from Equation 3.10 to the Laplace domain using

$$H(s) = C(sI - A)^{-1}B + D, \tag{3.11}$$

where I is the $2x2$ identity matrix.

Depending on what operating point is chosen, the transfer function $H(s)$ differs. The operating point vector was chosen based on the steady state temperatures that a certain set of PWM duty cycle and PWM period time yielded. In order to as accurately as possibly capture the complete spectrum of the nonlinearity within the linear model, a total of 15 transfer functions were calculated over three period times and five duty cycles. In other words for each chosen period time, five different duty cycles result in 15 different transfer functions. The transfer functions are seen in Table 3.3.

Table 3.3: Transfer functions and the corresponding PWM period times and duty cycles.

	10 s	50 s	100 s
100 %	$\frac{-10.02}{(40.02s+1)(716.35s+1)}$	$\frac{-10.02}{(40.02s+1)(716.35s+1)}$	$\frac{-10.02}{(40.02s+1)(716.35s+1)}$
90 %	$\frac{-10.56}{(41.31s+1)(720.56s+1)}$	$\frac{-10.76}{(41.68s+1)(721.56s+1)}$	$\frac{-7.43}{(40.23s+1)(694.44s+1)}$
50 %	$\frac{-11.98}{(43.54s+1)(727.27s+1)}$	$\frac{-20.20}{(54.29s+1)(760.63s+1)}$	$\frac{-25.05}{(54.70s+1)(757.58s+1)}$
20 %	$\frac{-15.29}{(48.38s+1)(741.73s+1)}$	$\frac{-46.96}{(74.84s+1)(839.63s+1)}$	$\frac{-65.82}{(75.47s+1)(869.57s+1)}$
5 %	$\frac{-16.83}{(52.20s+1)(753.91s+1)}$	$\frac{-145.83}{(92.03s+1)(925.44s+1)}$	$\frac{-141.23}{(92.51s+1)(1019.37s+1)}$

4

Barrel Temperature

In this chapter, the temperature in the barrel is simulated over time and the results discussed. In Matlab the simulations were run on the nonlinear model presented in Equation 3.6 while the linearized model from Equation 3.9 were simulated in Simulink. Therefore, this chapter is naturally divided into two sections - one for the Matlab results and one for the Simulink results. Before presenting the results, however, the expectations of the simulations are presented.

4.1 Expectations

Before showing the results of the simulation and beginning to analyze it, a hypothesis of what was supposed to happen is presented briefly.

When there are no molten plastic in the system, i.e., when there are no process disturbances, the temperature of the barrel is expected to drop to the ambient temperature of the room in which the system is located. The speed or ratio at which the temperature drops depends on whether the centrifugal fan is active or not. Of course, with the fan active the temperature is expected to drop faster than when the fan is off.

The same expectations hold for a system with process disturbance, with the difference being that the temperature equilibrium is no longer at ambient temperature but rather in between 210 °C and T_{amb} °C. What the temperature equilibrium should be is difficult to assume on before hand, as it depends on the properties of the plastic, and also how much cooling is applied. Either way, the equilibrium is expected to be between $100 - 150$ °C.

When a controller is applied to the system, the temperature of the barrel is expected to be controlled towards a given setpoint. The system is expected to respond to a setpoint change from $210 \rightarrow 160$ °C, i.e., a -50 °C change, and stabilize in about 10-15 minutes.

4.2 Nonlinear Model

By combining and rewriting Equation 3.6 from Chapter 3, one receives the dynamics of the temperature in the barrel as,

$$\dot{T}_b = \frac{1}{m_b c_b}(U_{b/p}(T_p - T_b) + d), \tag{4.1}$$

where

$$T_p = \frac{1}{U_{b/p} + U_{p/amb} + \dot{m}c_a}(U_{b/p}T_b + \dot{m}c_a T_{ambient} + U_{p/amb}T_{amb} - m_p c_a \dot{T}_p).$$

In this case $U_{i/j}$ denotes $A\alpha$ for the different heat transfer coefficient zones in Figure 3.12. Unless otherwise stated, the continuous, "real" airflow from Section 3.5 is used in simulations of the nonlinear model.

Since this is only the time derivative of the temperature, a method for creating the continuous temperature over time had to be produced. This was done discretely by iteration where the initial temperature was set to the predefined temperature of 210 °C. The next temperature could then be calculated using the previous temperature added with the temperature change for the matching time step provided by the expression in Equation 4.1. In other words, the barrel temperature over time is iterated as

$$\begin{aligned} T_b(i+1) &= T_b(i) + \delta_t \dot{T}_b(i), i = 0, 1, ...k, \\ T_b(0) &= 210\ ^\circ\text{C}, \end{aligned} \tag{4.2}$$

where δ_t is the time step and k is an arbitrary number of steps.

4.2.1 Without Process Disturbance

In this section, the process disturbance d is set to 0. Running the iteration seen in Equation 4.2 in combination with the model that is generating the airflow as well as the heat transfer coefficient model, the barrel temperature and its behaviour over time can be simulated.

During the initialization phase of this thesis, B&R presented a step response that had been performed on the real physical process. The only way to verify the Matlab model that this thesis results in is to compare its step responses with the one that B&R conducted. Figure 4.1 shows the reference step response as well as the corresponding step responses from the created model with 10 s, 60 s and 100 s PWM period time respectively.

The reference step response was performed on a system with no process disturbances, and its graph are showing both measured results (solid lines) and an attempt to fit a linear model (dotted lines) to the temperature. The reference shows how long time it takes for the temperature of the barrel to drop from 210 °C to 160 °C with different amount of cooling applied: 90 %, 50 %, 20 % and 5 % control signal. The system was tuned for the 90 % control signal case, which reached 160 °C in about 480 s.

The main point that is visible in the reference is the nonlinearity that B&R identified, and which also is the fundamental point of this thesis. If the barrel temperature behaved linearly in regards to the control signal to the fan, then the measured (solid) lines would appear on top of the dotted lines of the corresponding color.

After having built the model, described in the modelling Chapter 3, it had to be tuned in Matlab. This was done in the same way that B&R did, by applying a 90 % duty cycle to the fan. When the barrel temperature had decreased to 160 °C in 480 s using 90 % duty cycle, then the system parameters were finely tuned. The values of all parameters of the tuned model are available in Table 4.1.

After the tuning process was completed, the step responses for the other duty cycle percentages were simulated and presented in the same graph for reference. This was done for three different PWM signal period times: 10 s, 60 s and 100 s.

The temperature simulations of the 10 s period time case shows a step response where the temperature drops more or less equally fast no matter what duty cycle is used. This can be directly related to the earlier discussion about airflow controllability in regards to the PWM signal period time - a fast period time yields high average airflow output, and thus cooling effect, independently of the duty cycle.

In the simulation case with 60 s period time, the 90 %, 50 % and 20 % duty cycle step responses match the reference very well. The barrel drops in temperature too fast using 5 % duty cycle, and the reason behind this is unknown. Continuing, the last step response simulations were done on a system with 100 s PWM signal period time. Its results are similar to that of the 60 s case, with the main difference being that the temperature drops slightly slower.

These step responses indicate that a PWM signal period time of around 60 s is reasonable, and in comparison with the earlier airflow controllability discussions this makes sense logically.

The difference between the measurement and simulation results in B&R's reference step response is visually obvious, however the logic behind it is less obvious. If one analyzes the step responses of the model built in this thesis, the same nonlinearity effect is apparent between the 60 s and 100 s cases. One could argue that the

Table 4.1: Table of all system parameters.

Parameter	Description	Range	Selected value	Unit
t_{period}	PWM period time	1-100	50	s
B_{length}	Barrel length	-	0.3	m
R_{screw}	Radius screw	-	0.14	m
R_{inner}	Barrel inner radius	-	0.15	m
R_{outer}	Barrel outer radius	-	0.1754	m
R_{pipe}	Pipe radius	-	0.3	m
$T_{ambient}$	Ambient temperature	-	23	°C
T_{in}	Temperature plastic entering	-	210	°C
$T_{plastic}$	Average plastic temp	-	185	°C
$\dot{m}_{max}$	Maximum airflow	-	0.0732	m^3/s
C_p	Specific heat capacity plastic	-	1670	$J/(kg \cdot K)$
C_b	Specific heat capacity barrel	-	511	$J/(kg \cdot K)$
C_a	Specific heat capacity air	-	1012	$J/(kg \cdot K)$
$H_{airFree}$	Free convection air	2.5-25	17	$W/(m^2 \cdot K)$
$H_{airForced}$	Forced convection air	17-200	17-200	$W/(m^2 \cdot K)$
$H_{plasticForced}$	Forced convection plastic	100-500	100	$W/(m^2 \cdot K)$
k_{steel}	Thermal conductivity steel	16-24	20	$W/(m \cdot K)$
$k_{aluminum}$	Thermal conductivity aluminum	16-240	205	$W/(m \cdot K)$

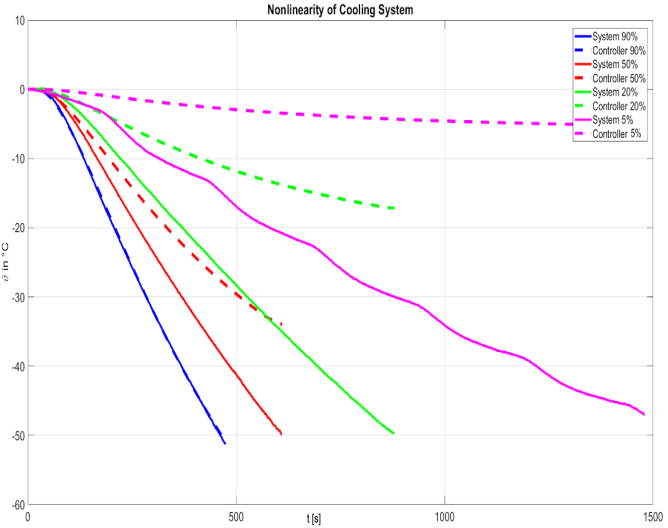

(a) Measurements provided by B&R, see Figure 1.5.

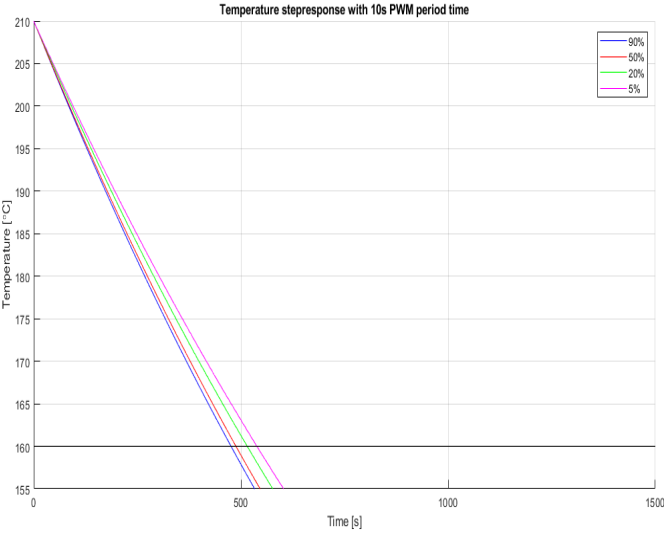

(b) Step response using 10 s PWM period time.

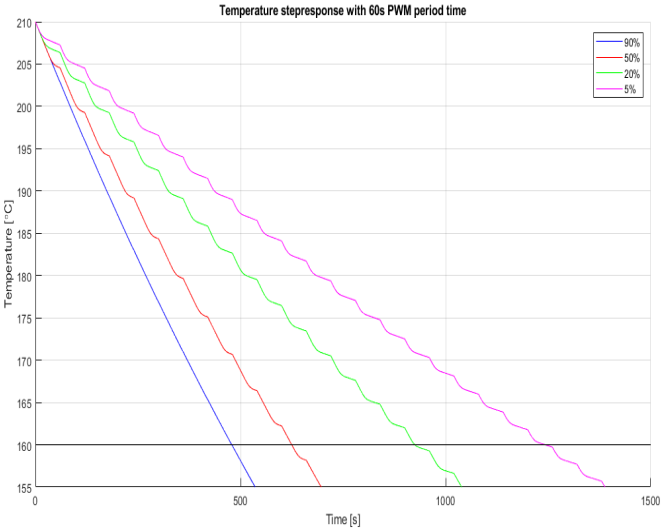

(c) Step response using 60 s PWM period time.

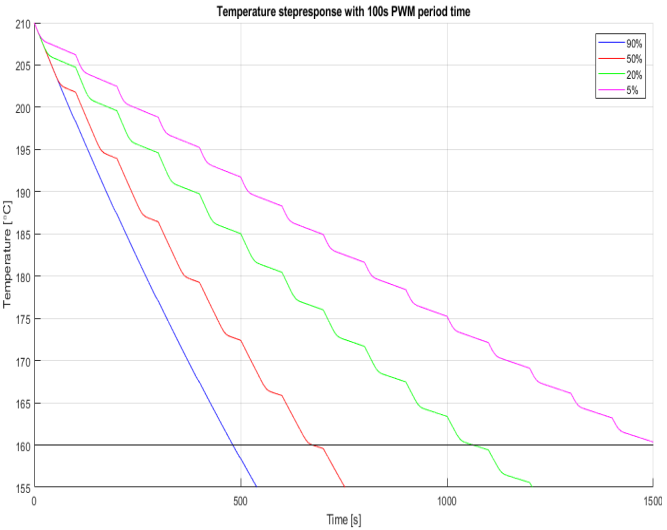

(d) Step response using 100 s PWM period time.

Figure 4.1: Step responses performed with different PWM period times and without process disturbance.

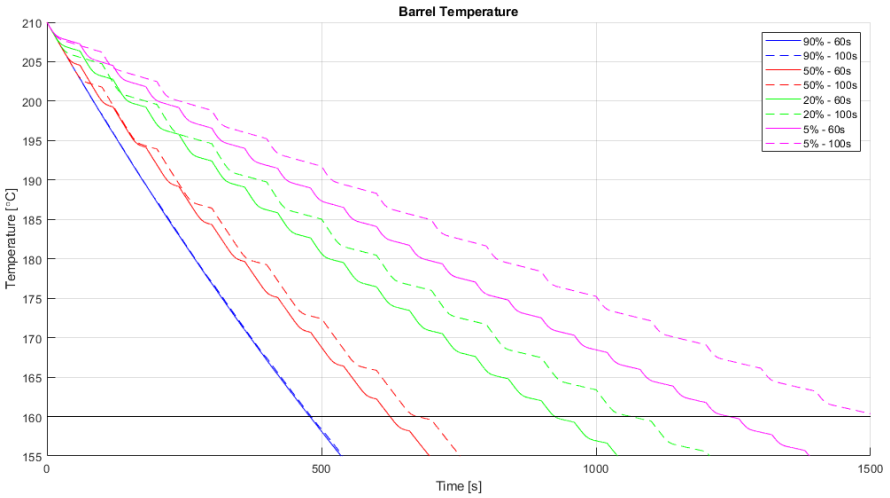

Figure 4.2: Step response comparison, 60 s period time vs 100 s period time.

difference between B&R's measurements and linear model are similar to the difference between a 60 s and 100 s period time in the thesis model. This is a reasonable implication that the nonlinearity has been identified and that it depends on the period time of the controlling PWM signal. As mentioned earlier, the period time is strongly correlated to the airflow output, and the relation between average airflow and PWM duty cycle becomes more linear with a longer period time. For the sake of argument, Figure 4.2 shows the difference between the 60 s case and the 100 s case. If the period time would be increased even further, for example to 1000 s, the relationship between the average airflow and the duty cycle is basically linear, see Figure 4.3. This would correspond to more or less full controllability of the airflow, which in turn controls the cooling effect. Naturally, this effect is desirable but a 1000 s period time is totally unrealistic due to the fact that the system responds to a 50 °C setpoint change in 600 seconds, which is demonstrated later.

Figure 4.4 shows the simulation results for different airflows and PWM duty cycles for three different period times: 1 s, 10 s and 100 s. Clearly there is a significant difference in the barrel temperature behavior for low duty cycles between the 100 s period time and the 1 s or 10 s period times. Through this simulation it can be concluded that the period time with which the PWM signal is cycled will make a noticeable impact primarily on the low end of the control spectrum, whilst running the cooling fan at 100 % will always correspond to the maximal airflow no matter what period time is used. This also explains the curves being stacked on top of each other in the last subplot containing the data from the 100 % duty cycle test.

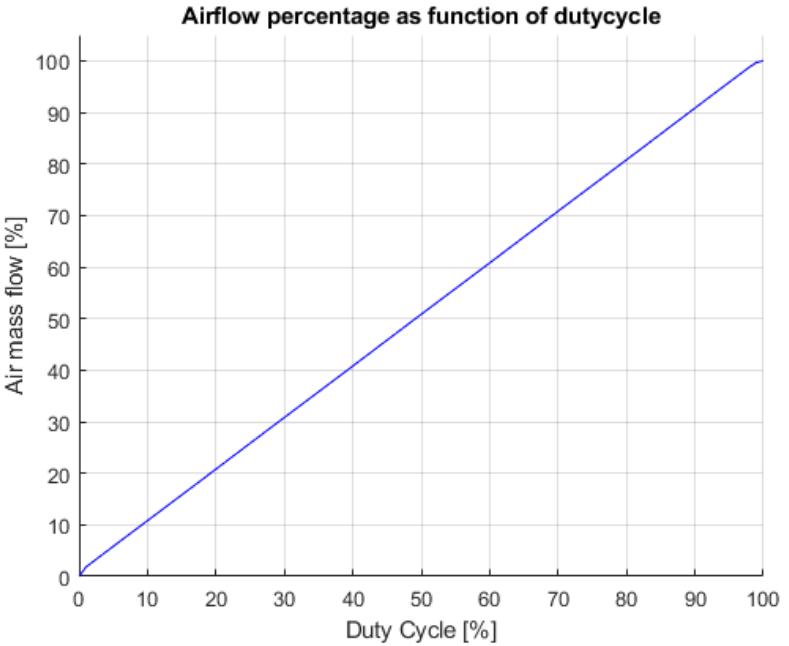

Figure 4.3: Relative airflow output as function of duty cycle for a period time of 1000 seconds.

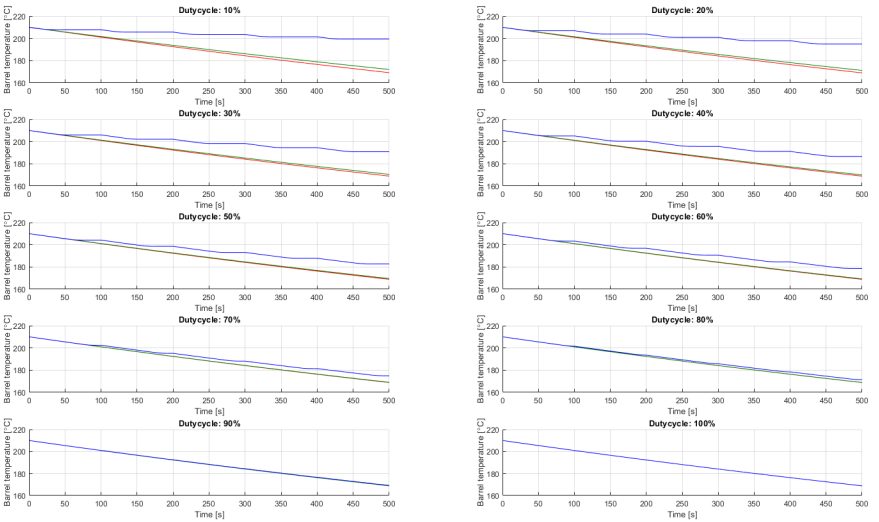

Figure 4.4: Temperature decrease in barrel over time without a disturbance. Duty cycles from 10 % to 100 %. *Red* using a PWM signal with a period time of 1 s, *Green* using a period time of 10 s and, *Blue* using a period time of 100 s.

Another thing worth mentioning here is that the dimensions of the process will have a large impact on how the temperature changes over time. The current dimensions have been carefully chosen to get a similar temperature response as the provided step response measurements seen in Figure 4.1a provided by B&R. The dimensions seem reasonable according to logic and eye measurements but it is unclear how close or far away the sizes are from the real machine. The main concern is the active cooling surface interfacing the barrel and airflow - this otherwise lateral surface area of the cylinder shaped barrel is covered with cooling fins of which the area is unknown. Estimations have been made concluding that the area is probably somewhere between 2-4 times larger using fins than the original lateral surface area.

Startup differences between model and reality A substantial difference can be seen in the beginning of the step response that B&R provided and the simulated step response. When looking at the initial temperature decline behaviour of the provided step response it can be seen that after applying cooling it will take some time before it starts to affect the measured temperature. This is not the case in the simulations where the temperature immediately starts to decline rapidly after applying cooling. At first it was believed that this was due to the barrel having inaccurate size or other faulty material specific properties. It would make sense that a larger solid iron/steel construction would have a much greater "thermal inertia", thus taking longer time to cool down after being heated.

The effects of changing the size and density parameters were tested but the same direct temperature decrease was observed no matter what settings. The reality of it is that the energy equilibrium model used is a simplified model of reality. As mentioned in Chapter 1 it was preferred by B&R to create a simplified model and to refrain from developing complex differential Equations to describe the temperature at every single point and time in the system. By removing the position aspect/dimension from the Equations entirely, one could possibly mess with the perception of the overall temperature. Therefore the main reason for the delayed temperature response is believed to be that the temperature of the simulation is calculated assuming that the temperature is uniformly distributed within the barrel at all times. The reality of it is that during cooling the edges of the cooling fins furthest away from the plastic channel should be the coldest and then the temperature will increase as it gets closer and closer to the inner wall of the barrel.

The real measurements were taken using a thermal coupler positioned half an inch inside of the barrel wall, in other words closer to the inner wall of the barrel. Therefore it stands to reason that it would take some time before the temperature of the material surrounding the sensor starts decreasing significantly. This also would imply that the overall temperature will continue to decrease even after the cooling is turned off completely. This should continue until the barrel temperature has stabilized and the temperature is more or less the same all throughout the barrel once

again. A delayed response could most certainly be added to the model, but as of right now it is deemed enough to know about this complication that is created by the simplifications.

By linearizing the nonlinear system around certain working points, the difference in startup behaviour may be eliminated. This will be discussed at a later stage in the thesis.

Temperature Equilibrium As proposed in the expectations section, Section 4.1, it is expected that the barrel temperature drops over time and stabilizes at room temperature when there is no process disturbance involved. Figure 4.5 shows that the barrel temperature indeed drops over time and stabilizes at room temperature independently of whether cooling is applied or not. The rate at which the temperature drops depends on the amount of cooling applied, and Figure 4.5 clearly demonstrates that 100 % cooling results in the fastest temperature drop, while 0 % (passive) cooling requires more time to stabilize. This validates the physics behind the model, and confirms that it behaves as expected. The rate of which the barrel temperature drops depends on both the applied cooling and the dimensions of the system.

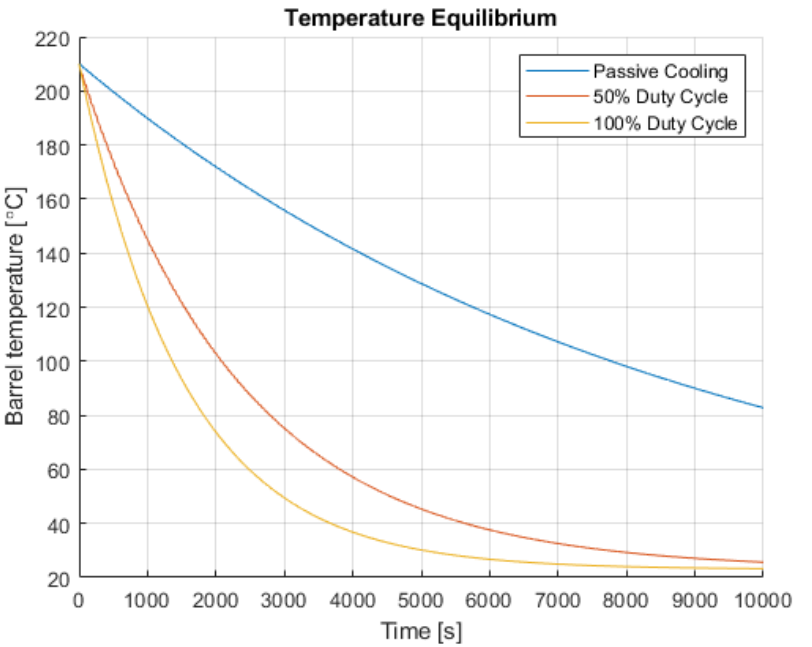

Figure 4.5: Barrel temperature equilibrium without process disturbance.

Average vs Continuous Airflow Using the continuous airflow model described previously should generate the best results since it should represent reality. However for the sake of simplicity say that the average airflow for the corresponding duty cycle was used instead. How would this effect deviate from the real airflow? The reason for this being researched is that this could be used to map a specific control signal to a specific airflow and thus compensate with this value when running the fan controller with a faster PWM signal.

This should generate similar results as to using the real airflow.

Real airflow referrers to the PWM alike behaviour previously seen Figure 3.8, where the airflow can be everything from $0 - 100$ % at any given time. Average airflow referrers to an average airflow calculated at each duty cycle seen previously in Figure 3.9.

It is primarily at low duty cycles the difference over time will become substantial, the temperature difference over time can be observed in Figure 4.6 below.

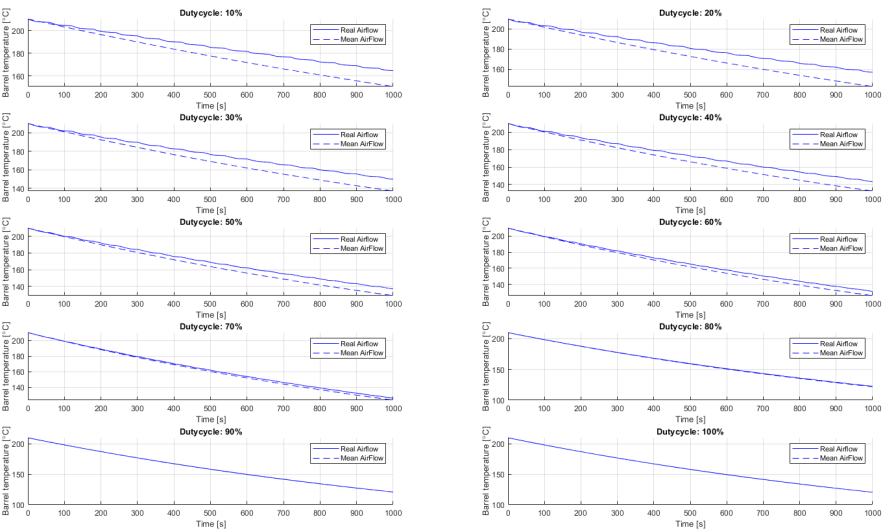

Figure 4.6: The temperature over time using real and mean airflow.

4.2.2 With Process Disturbance

In this section, simulation results where the process disturbance is present is provided. This means that by now, the process and the model has been tuned with satisfactory results and step responses, and it is ready to be tested with molten plastic present. A PI controller is designed and tuned using *lambda tuning* [*Fundamentals*

of lambda tuning 2021] in order to control the system with disturbance present.

Temperature Equilibrium As a method of verification, similar to what was done without disturbance, the barrel temperature equilibrium is checked. As per the expectations subsections, the barrel temperature is expected to stabilize at a temperature of about 100 °C to 150 °C. Figure 4.7 shows that the barrel temperature stabilizes at around 154 °C using a heat transfer coefficient of the plastic of 450 $\frac{W}{m^2K}$ with 100 % cooling applied. 154 °C was deemed a bit too high and unrealistic after discussions with the B&R supervisors, as this means that with 100 % cooling the barrel temperature would differ just 6 °C from its setpoint value. If that was the case, then having a controller for the cooling would not be necessary as the ceramic heating bands, which already have accurate controlling, could add a little heat to minimize the error.

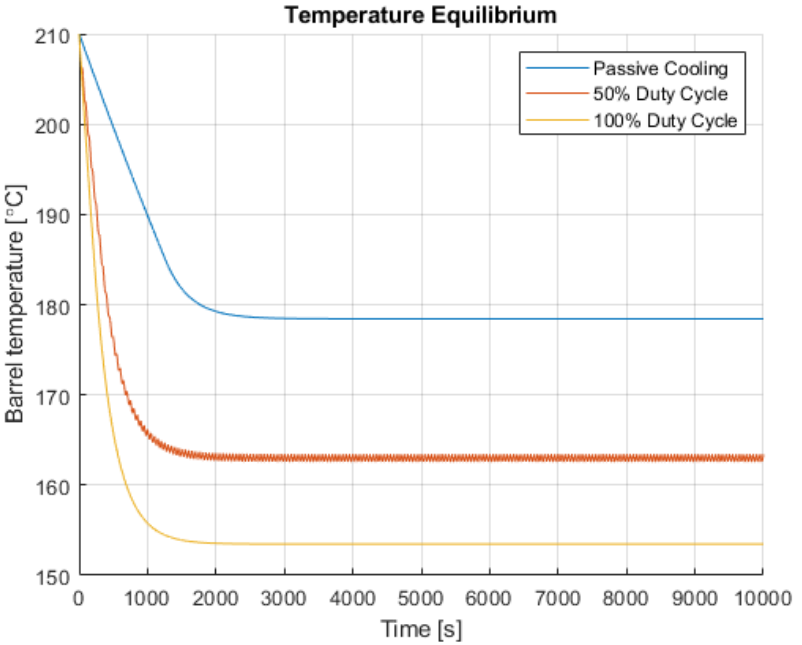

Figure 4.7: Barrel temperature equilibrium with process disturbance and plastic heat transfer coefficient of 450 $\frac{W}{m^2K}$.

The heat transfer coefficient for the plastic was thus changed to 100 $\frac{W}{m^2K}$, and the results of this is demonstrated in Figure 4.8. Now the temperature stabilizes at 112 °C, which is more realistic. The figure also demonstrates that the amount of cooling applied effects the temperature equilibrium. If a more powerful centrifugal fan was

available, or if the dimensions of the system were changed, then the equilibrium could potentially be pushed towards the ambient room temperature.

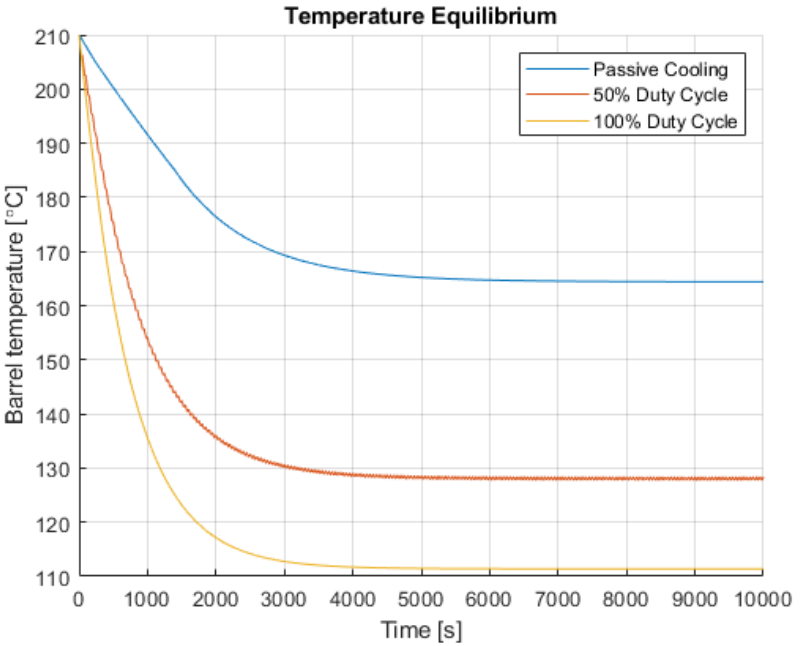

Figure 4.8: Barrel temperature equilibrium with process disturbance and plastic heat transfer coefficient of 100 $\frac{W}{m^2K}$.

PI Controller The discrete PI controller was initially designed and configured to run on the same frequency as the PWM fan controller, since nothing could be done in terms of changing the control signal during a period. It was however later discovered that the controller was running a bit smoother if it was allowed to do calculations at a higher frequency. This is due to the fact that it constantly has access to reading the barrel temperature sensor, and then is able to adjust its values accordingly to output the best control signal when a change was allowed.

Lambda Tuning The controller was tuned using lambda tuning, which is an internal tuning method that endows a PI controller the ability to generate smooth, non-oscillating control signals when responding to setpoint changes [*Fundamentals of lambda tuning* 2021].

Lambda tuning is a method which builds on a step response experiment, through which the static amplification or process gain K_p, dead time L_D and time constant T

of the process is determined according to Figure 4.9. The process gain is given by

$$K_p = \frac{\Delta y}{\Delta u}. \tag{4.3}$$

A tangential line is drawn through the point at which the slope is the steepest, extended to the level at which the process variable was before the step occurred. The dead time is defined as the time that passes between the step occurring and the intersection of the tangential line and the original level of the process variable. The time constant is defined as the time it requires for the process variable to reach 63 % of its total change from the intersection at the end of the dead time. The PI control parameters K and T_i are then given by

$$\begin{aligned} K &= \frac{T}{K_p(L_D + \lambda)} \\ T_i &= T, \end{aligned} \tag{4.4}$$

where $T \leq \lambda \leq 3T$ decides the speed of the controller. A small value of λ corresponds to a faster control loop while a larger value yields a slow closed-loop response. λ could potentially be chosen smaller than T, but that may generate some oscillations which means that the main objective of the tuning is lost.

Attempts to Control the Model The cooling system is running with a PWM controller, configured for a 60 s period time as per previous discussions. The PI controller output its control signal at the same frequency. With the current tuning, a setpoint change of -50 °C will result in the proportional part of the controller saturating the control signal during the initial part of the temperature change. This leads to fast responses which keeps the fan running at 100 % for as long as the controller deems it necessary. When the majority of the setpoint change has been accounted for, the integration part will take over and remove the, otherwise stationary, error using smaller control signals.

In Figure 4.10 it is possible to observe the temperature and control signal behaviour resulting from a well tuned PI controller. In about 600 s, the controller responds to and controls the temperature of the barrel to the setpoint value of 160 °C, provided that the temperature starts at 210 °C. In Subsection 4.2.1, the delayed startup behaviour and a difference between the model and the reality was discussed. A result of this difference is that this response probably is too quick compared to what it should be. Thus, for the simulation to be more fair, it can be concluded that the final time for the setpoint change can be set to around 630 s instead of 600 s. For reference another setpoint of 146 °C is chosen in Figure 4.11 to illustrate a more stable control signal after the set temperature is reached.

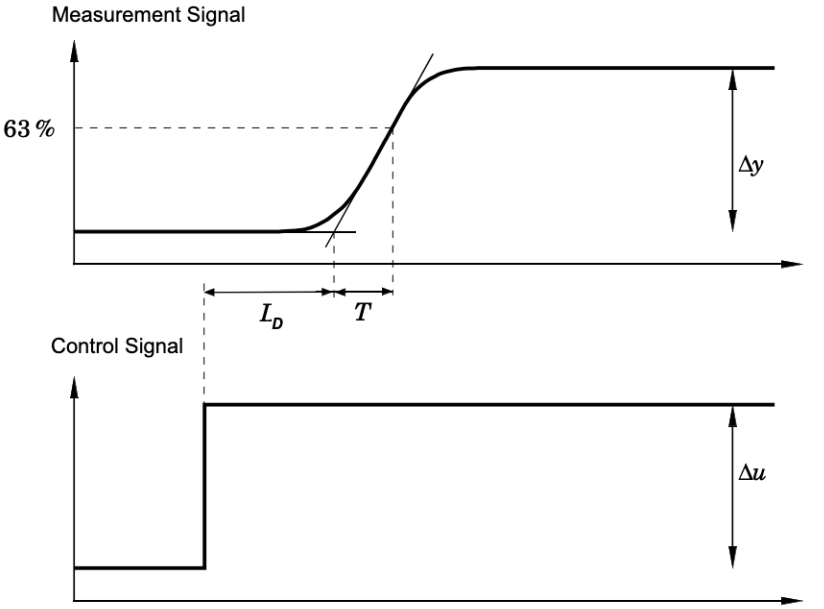

Figure 4.9: Lambda tuning method [Department of Automatic Control, 2021].

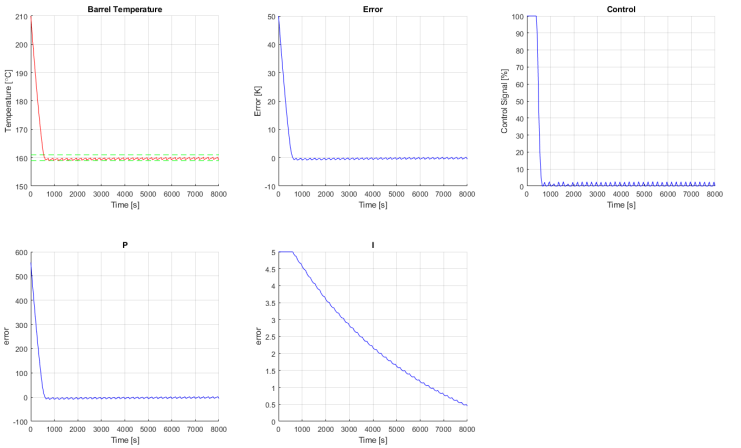

Figure 4.10: PI controller responding to a setpoint change to 160 °C.

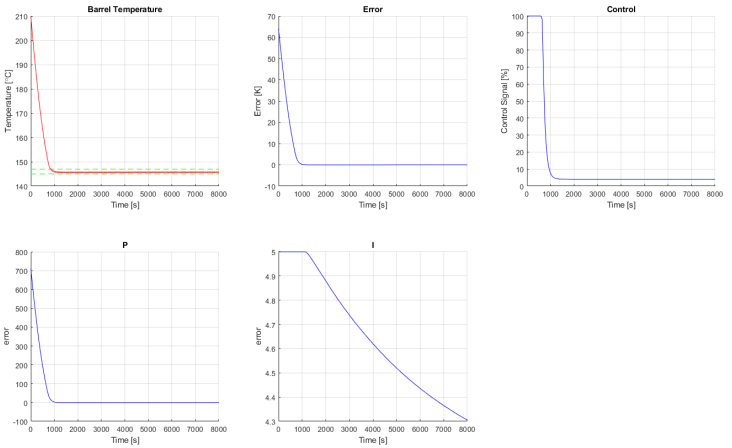

Figure 4.11: PI controller responding to a setpoint change to 146 °C.

For reference, B&R has provided data form a similar setpoint change that was performed on the real physical process using a PID controller, see Figure 4.12. In this figure, it is a bit difficult to visually see the axes due to poor image quality and the fact that the setpoint change does not happen at time $t = 0$. To cope with this B&R manually shows that it takes about 660 s for the process to stabilize at the new setpoint temperature.

Apparently, the simulations of the model created in this thesis matches the reality provided by B&R quite well. It is, however, difficult to conclude whether the model is reliable to a high extent due to the large parameter and dimension uncertainties described earlier.

Random Noise For the sake of stability, Figure 4.13 demonstrates what happens to the barrel temperature when some minor but random noise is added to the temperature measurements. The same tuning parameters were used as in the previous case. As mentioned earlier the temperature is being generated discretely, therefore to accomplish variations in the measurements a random value between -0.03 and 0.03 are added to the temperature at each time step. This is to simulate the overall effect of a noisy temperature sensor reading.

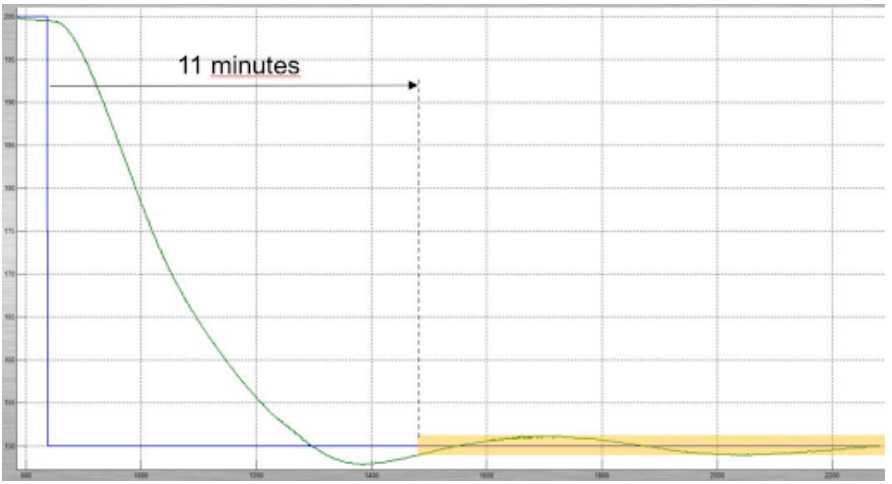

Figure 4.12: PID controller responding to a setpoint change on the real process, provided by B&R.

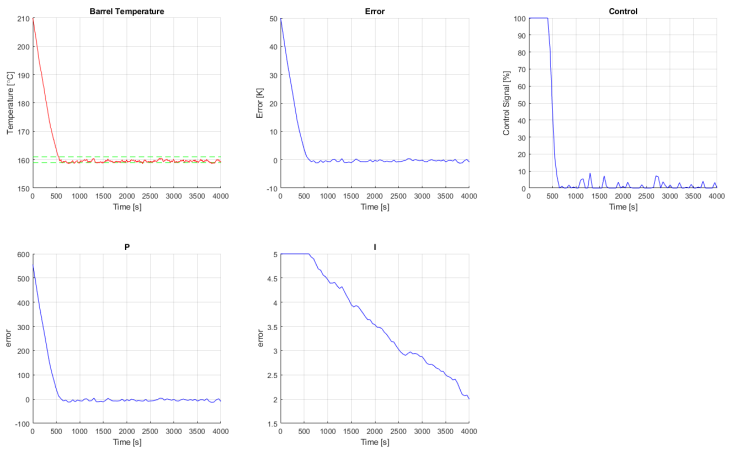

Figure 4.13: PI controller responding to a setpoint change with some noise.

4.3 Linearized Model

The linearized transfer functions from Table 3.3 were set up in a Simulink environment, see Figure 4.14, for an example, for all duty cycle cooling percentages and PWM period times to be simulated in regards of step responses. The main reason as

to why it was requested that the nonlinear system was to be linearized was to verify that the dynamics of the process matches the data provided by B&R. As mentioned earlier, the step responses that were simulated in Matlab have a startup behaviour that differs from the typical S-shape that comes from systems with transfer functions on the form $H(s) = \frac{K}{(sT_1+1)(sT_2+1)}e^{-T_3 s}$. Thus by linearizing the system, comparing the resulting transfer functions with B&R's and analyzing the step responses of the linearized system the dynamics could be verified. For the simulations on the linearized model, the average airflow from Section 3.5 is used.

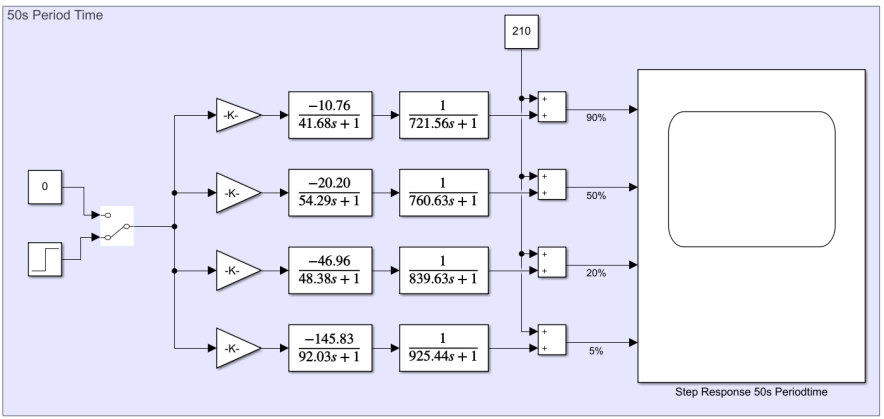

Figure 4.14: Simulink environment for simulating step responses on the linearized system. In this example the PWM period time was set to 50 s. Similar environments are set up for the 10 s and 100 s period time cases.

By running the Simulink simulation, the scope view captures the linearized transfer function responses when an input step occurs. For convenience, the step responses for the different PWM period times are shown in the same figure together with B&R's reference response, see Figure 4.15.

The initial observation that was made from these step responses was that simulating a 100 % duty cycle control signal to the centrifugal fan resulted in the same response independently of what PWM period time was chosen. In comparison to the reference, the 100 % cooling case also looks reasonable even though B&R's 100 % cooling cools faster, due to the reference not taking process disturbance plastic into consideration which slows the temperature drop down. It is also clear that a longer PWM period time means more controllability, but that has already been discussed.

Furthermore, the step responses demonstrate simulation times that take slightly longer to reach 160 °C then that of the responses from Matlab. The reason for this

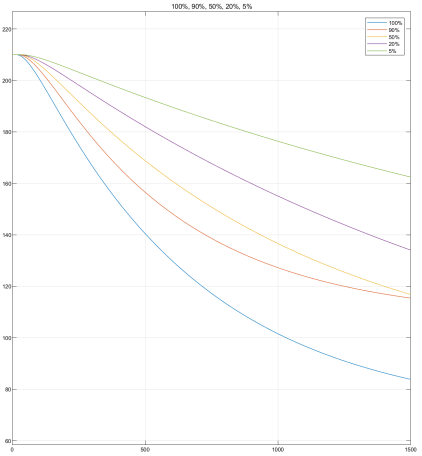

(a) Reference.

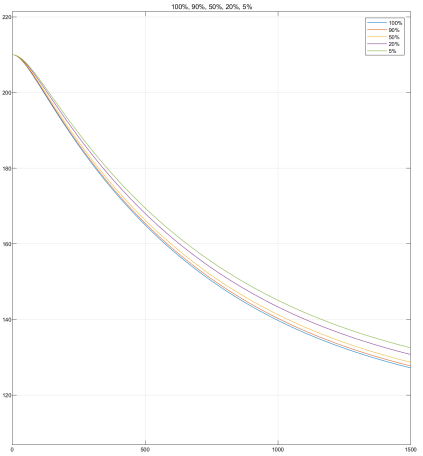

(b) 10 s period time.

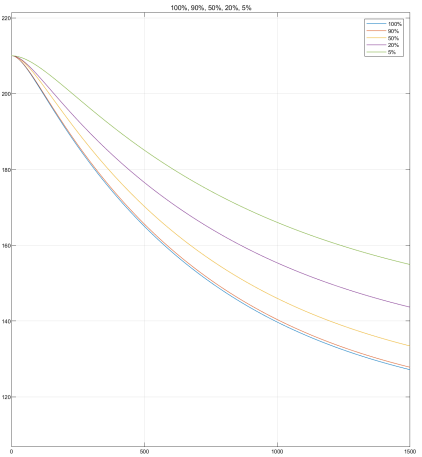

(c) 60 s period time.

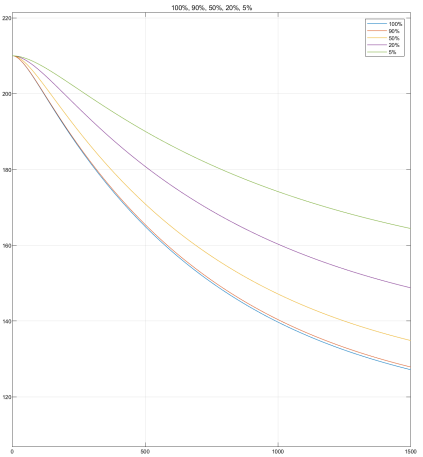

(d) 100 s period time.

Figure 4.15: Step responses of the linearized transfer functions, simulated in Simulink.

is probably that the linearization far away from the chosen operating points is not as accurate as the nonlinear model, thus the times may differ slightly.

In Figure 4.16, a comparison between the Matlab script that contains the nonlinear model and the Simulink environment that holds the linearized model is shown. It is possible to visually determine a 30-60 s difference in time to reach 160 °C between the 100 % duty cycle cooling cases. As mentioned in the previous paragraph, it may depend on the fact that the linearized model lacks accuracy far away from the operating point. However, it is also clear that the linearized transfer function contributes to the S-shaped response curve that, according to earlier discussions in the thesis, describes the dynamics of the system in a way that is more accurate in the real life physics outside of the simulation environments. A conclusion to be drawn from this is that the combination of the fact that the linearized model behaves similar enough to the nonlinear model and that its startup behaviour is superior makes the linearized model valid.

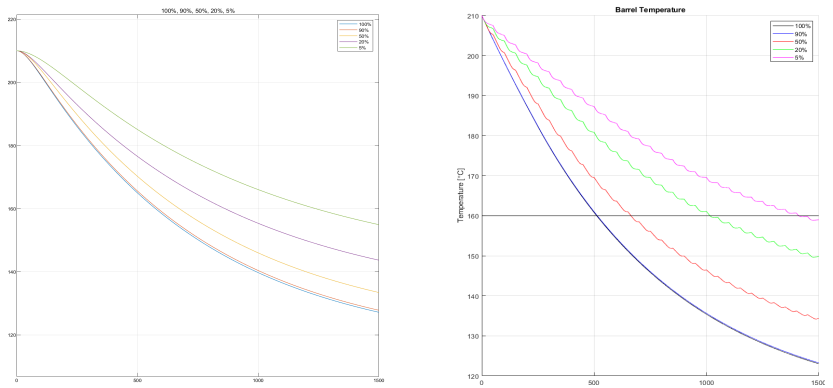

(a) Linearized model. (b) Nonlinear model.

Figure 4.16: Difference between linearized model and nonlinear model, with a PWM period time of 50 s.

4.3.1 PI Controller

Now that the linearized transfer functions are validated through step responses, a PI controller has to be built to control the system towards a reference setpoint. The theory behind the controller remains the same as for the Matlab environment, however Simulink offers a configurable built-in PID controller as a part of a standard library. For simplicity, this controller was used and configured as a PI controller.

Due to the fact that the system at this point was linearized around the process' equilibrium points which are far away from the initial condition value, two separate controllers were implemented, see Figure 4.17. The first controller, *startup con-*

troller, had the purpose of controlling the system from its initial value of 210 °C to roughly 160 °C in a non-aggressive way. The purpose of the second controller, the *steady-state controller*, was to control the system more aggressively close to the reference setpoint to be able to handle disturbances and process variations. In Figure 4.17, the PWM period time is set to 50 s. The linearized transfer function of the 50 % duty cycle case was chosen as the average transfer function, and therefore considered most appropriate to use as the process in the control structure. Note that the linearization subsequently introduces errors when the temperatures are far away from the chosen operating points.

In the Simulink environment, for simplicity, the swap between the two controllers was time based. In reality, if this control structure was to be implemented, the condition for changing controller would have to be finely tuned and based on the control error instead of time.

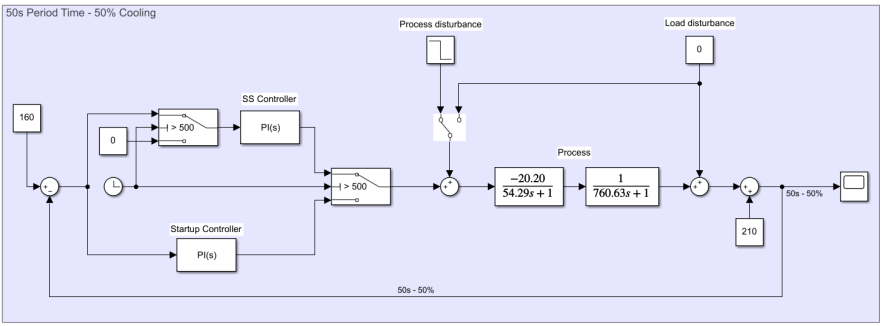

Figure 4.17: Control structure consisting of two PI controllers used to control the linearized system in Simulink.

After tuning the PI control structure through "trial and error" the system responded well to setpoint changes. It was also possible to handle process disturbances, see Figure 4.18. It can be seen that it takes about 500 s for the system to reach and stabilize around the setpoint of 160 °C when starting at 210 °C. After 1000 s, a process disturbance is applied in the form of a step. The disturbance is handled quickly with no issues.

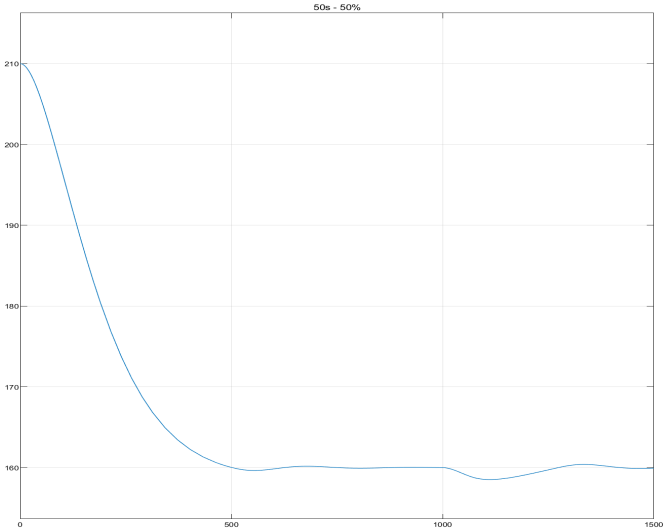

(a) System response.

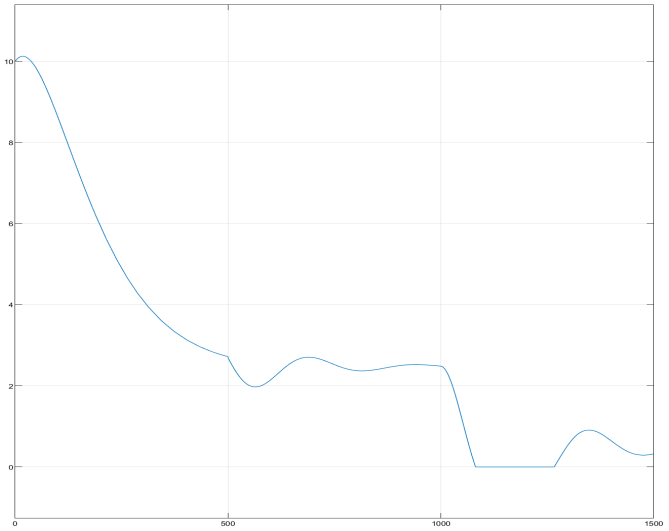

(b) Control signal.

Figure 4.18: System responding to a setpoint change using the PI control structure. A disturbance is added after 1000 seconds.

5

Improvements & Suggestions

5.1 Flow manipulation

Up until this point, everything has been based around controlling the fan and trying to optimise the generated airflow to achieve similar results as given data of the real process. It has also been concluded that the root cause of the regulation problems occurring is the stored inertia in the fan/motor assembly. If there was a way of minimizing the ramp down time most of the problems would be resolved. By shortening the time taken for the fan to make a complete halt, the airflow would look more like the control signal sent to the motor relays. The more alike this signal the airflow becomes, the easier it is to control the cooling more precisely. In other words, the same controllability effects that increasing the period time of the PWM signal would result in, can be caused by manipulating the airflow in other ways.

Figure 5.1 shows what happens to the delivered airflow as a function of duty cycle of the PWM signal when the ramp down time is reduced to 10 s and 0.5 s, compared with the original 30 s. With this figure in combination with Figure 5.2, it becomes clear that the faster the fan ramps down, the more controllable the airflow becomes. The linear controllability that one supposedly would have if using an unrealistic period time of 1000 s, see Figure 4.3, is thus achievable by making the fan stop faster.

Improved controllability is not the only thing that a faster ramp down time would yield. If the fan stops faster then the period time of the PWM signal could be reduced, which in turn would reduce the oscillations caused by a high period time. Figure 5.3 demonstrates the oscillations that are introduced to the system as a result of the PWM period time. In conclusion, reducing the ramp down time of the fan results in that the trade-off between controllability and oscillations become less relevant.

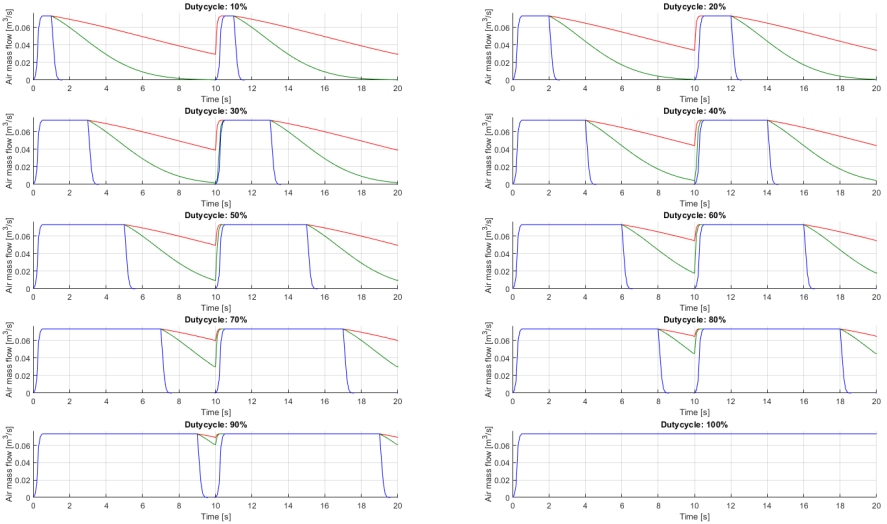

Figure 5.1: Airflow as a function of duty cycle with reduced ramp down times. The *red* graph shows the original ramp down time of 30 s, while *green* and *blue* shows the corresponding graphs for ramp down times of 10 s and 0.5 s, respectively.

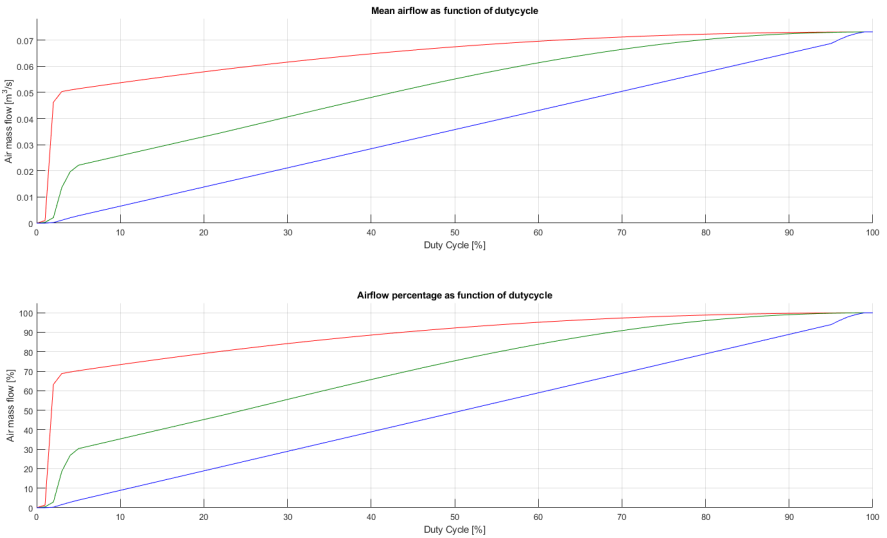

Figure 5.2: Average airflow as a function of duty cycle, PWM period time of 10 s. The *red* graph shows the original ramp down time of 30 s, while *green* and *blue* shows the corresponding graphs for ramp down times of 10 s and 0.5 s, respectively.

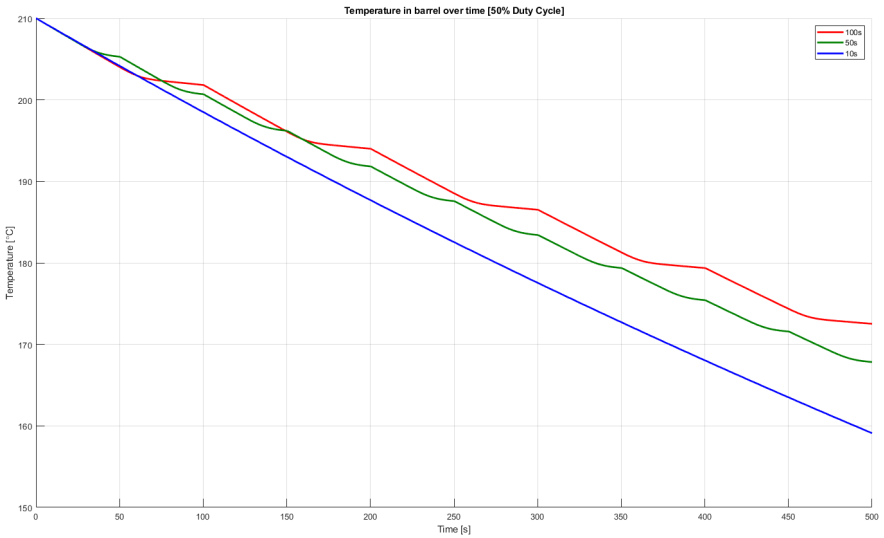

Figure 5.3: Barrel temperature over time with 50 % duty cycle cooling applied. The *red*, *green* and *blue* curves have PWM period times of 100 s, 60 s and 10 s, respectively.

As the effects of manipulating the airflow have been demonstrated, two alternatives on how to accomplish said manipulation is discussed - applying brakes or introducing flow valves.

5.1.1 Brakes

The first flow manipulation alternative is to apply brakes to the shaft of the fan that would slow it down and consequently reduce the airflow. The positives with this are already described, but not the negative aspects. This method naturally involves a lot of friction which would increase the wear and tear of the fan. Another disadvantage is that some sort of control algorithm needs to be developed for the brakes, which potentially increases the complexity of the system. In order to find the best possible brake solution, another project have to be conducted.

5.1.2 Valves

The second flow manipulation alternative is to introduce a flow valve in between the fan and the duct that surrounds the plastic extruder barrel. By opening and closing this valve the airflow could be regulated quite well. However, one aspect is that the air pressure will increase with a partially opened or closed valve. In terms of efficiency, this alternative is definitely better than brakes, but reducing the flow without

slowing the fan down would, in fact, put more strain on the motor, thus the power consumption may increase somewhat or even substantially.

This issue could possibly be resolved by using two valves - one connecting the fan to the barrel ducting and one connected to an outlet to the ambient environment. When controlling the main valve connected to the extruder, the secondary valve should mirror the inverse of the main valve. This would keep the pressure constant, but these kinds of solutions quickly adds a lot of complexity to the system.

5.2 Ways to get rid of nonlinearity

Altering the physical machine by adding brakes or valves is something that most customers would prefer not to do, mainly because it is more expensive to install and maintain but also because it adds mechanical complexity. Instead, what could be done, is to modify the software behind the controller. Two ways to do this are by *Gain Scheduling* and *Inverse Function Compensation*.

If no changes should/could be made to the physical machine it could be possible to use other methods to get rid of the nonlinearity by tweaking the controller. The preferred method would probably be to add gain scheduling to the system which is a method for changing the systems gain depending on what interval the control signal is within, thus compensating for the nonlinear behaviour. However there are also other ways, one of which is to invert the nonlinearity which in this case primarily is the airflow from the fan. By inverting the airflow as a function of control signal and then multiplying the newly created function with the corresponding control signal a linear behaviour will present itself.

5.2.1 Gain Scheduling

In theory, gain scheduling is a way to control a nonlinear system with a set of linear controllers that each focus on controlling the system satisfactorily over different operating points. A set of scheduling variables determine which linear controller should be active at a certain point in time. If the nonlinearity in Figure 5.4 is considered, then controlling this nonlinearity through gain scheduling would imply that three different linear controllers should suffice. One of the controllers would be active in each interval area, where the gains of the controllers should be chosen appropriately compared to its active region.

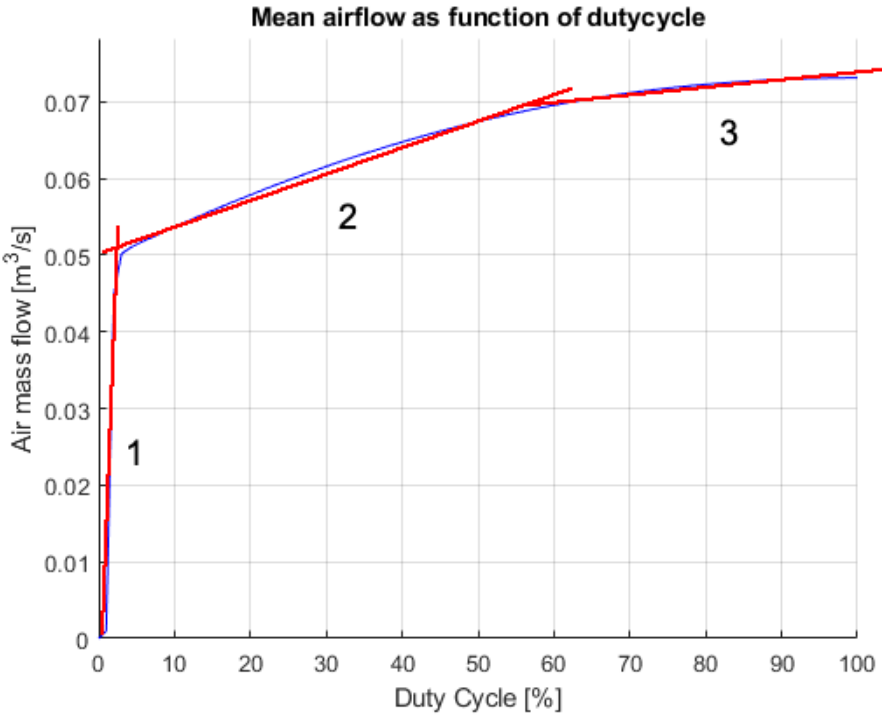

Figure 5.4: Gain scheduling with three regions applied to the airflows nonlinearity.

One could also argue that having one linear controller and instead vary the process could possibly be a valid option as well. An example of this is shown in Figure 5.5, where the linearized transfer functions from Table 3.3 make up the process variations. This, however, is far from ideal and presents a control problem that is difficult to tune.

5.2.2 Compensating with Inverse function

The second way to compensate for the nonlinearity that is covered in this thesis is by inverting the nonlinearity and incorporating it in the controller. In theory this would cancel out the nonlinearity completely, however it requires not only that the nonlinearity is nice and smooth, but also that it is invertible and can be describes as function. Again, consider the nonlinearity from Figure 5.5. This time, instead of applying gain scheduling to reduce the effects of the nonlinearity, it will be compensated by the inverse of the nonlinearity. Naturally, the nonlinearity has to be approximated by a function with as small of an error as possible to achieve reason-

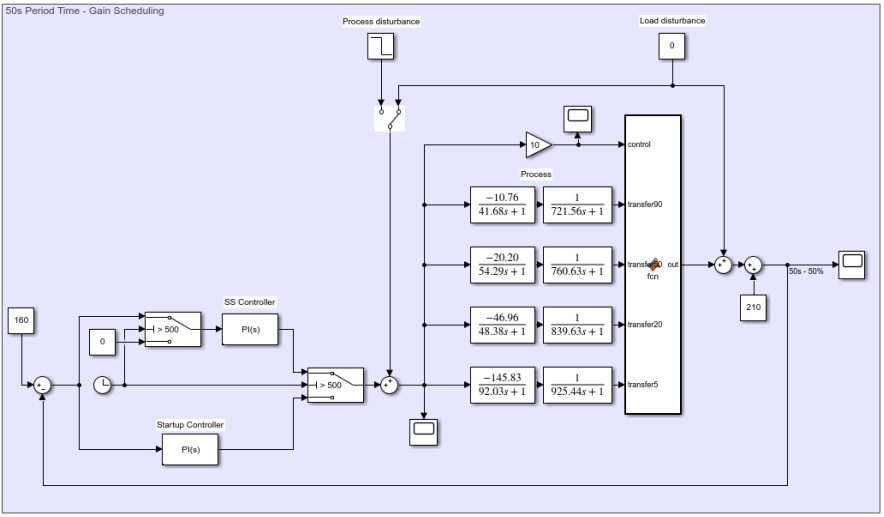

Figure 5.5: Gain scheduling example in a Simulink environment.

able results. Figure 5.6 shows a reasonable approximation of the nonlinearity using a logarithmic function.

In order to demonstrate the principles of reducing the effects of the nonlinearity, the approximated function is inverted and then multiplied with the original function. The results of this is visible in Figure 5.7, where it is clear that the result is linear. In reality, this method of nonlinear compensation is a bit more complex to implement, however that will not be discussed in this thesis.

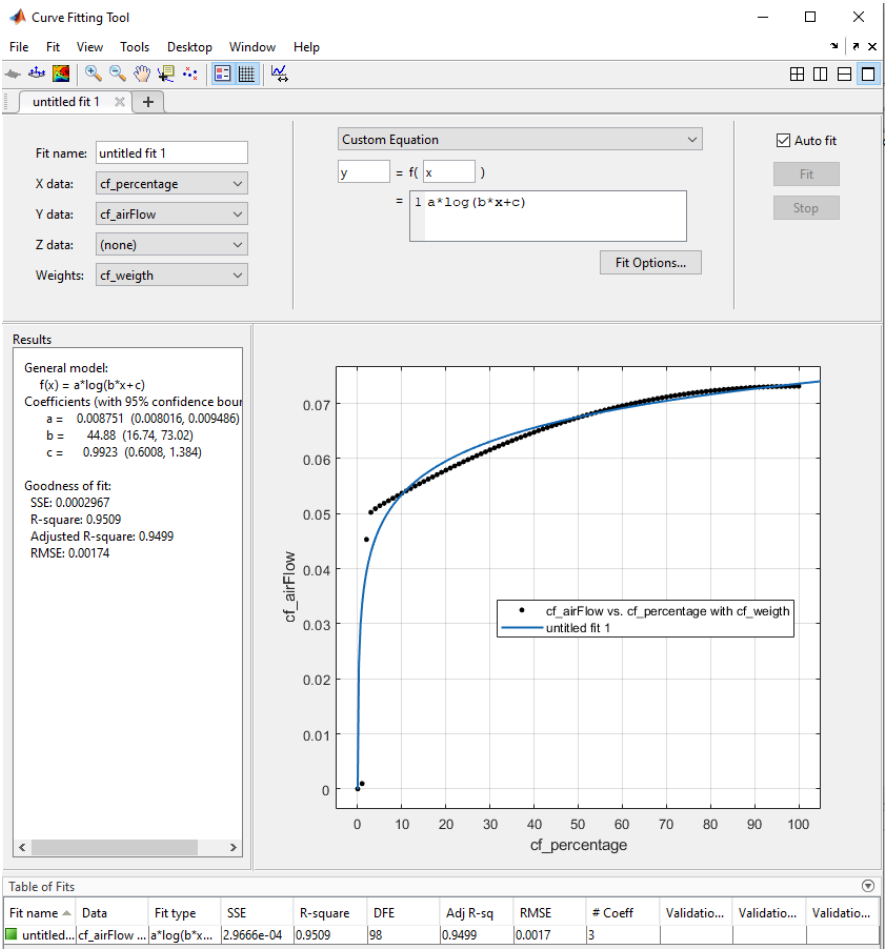

Figure 5.6: Approximation of a nonlinearity using a logarithmic function.

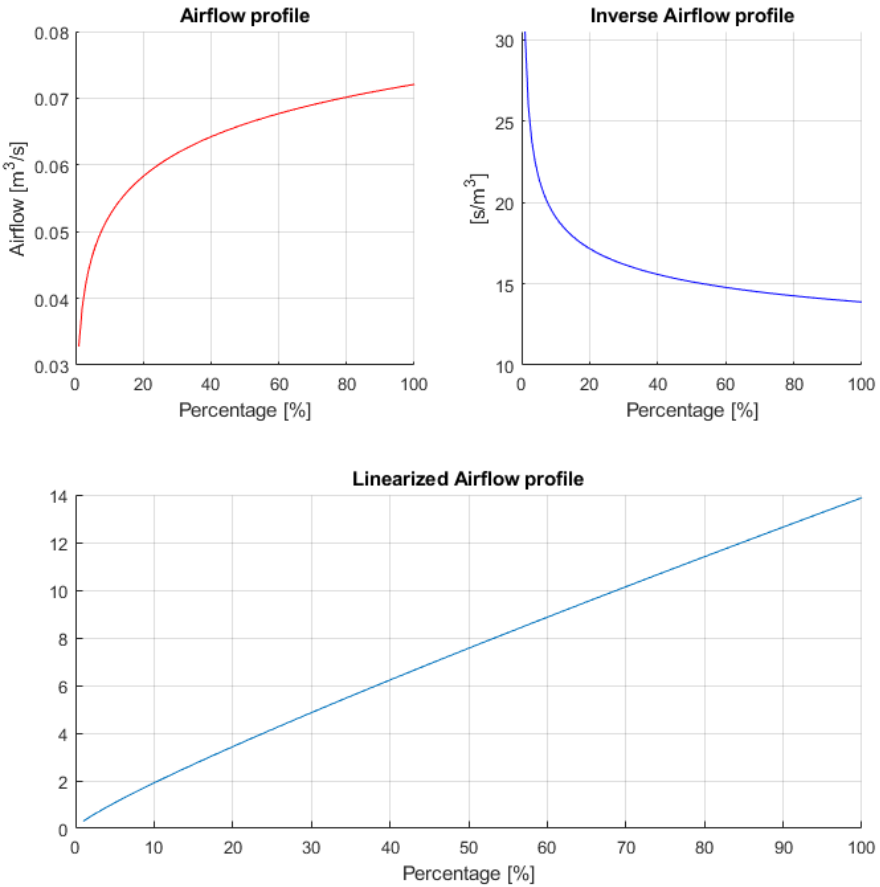

Figure 5.7: Demonstrating the principles of inverse function compensation of a nonlinearity.

6

Conclusions & Future Work

This thesis was conducted during the Covid-19 pandemic, which brought along a lot of challenges in terms of internal communication and meeting possibilities. Because of the pandemic, no possibilities to run tests on the physical process were presented which means that all results and discussions are theoretical and based on a thermodynamic model. The model parameters and dimensions have thus not been confirmed, which of course adds additional uncertainties to the achieved results.

Despite this, it may be concluded that the thesis project yielded insightful knowledge about the extruder cooling system and the nonlinear parts of it. Matlab and Simulink simulation models were built and alternative ways to improve both the physical system and the software based controller were discussed. The main cause of the nonlinearity was the dynamics of the centrifugal fan. With that stated, all objectives as stated in the introduction of the thesis are met.

Since the thesis work has been conducted in a theoretical environment using simulations as the only method of verification, there are potential future work to be done. This mainly includes performing tests on a real plastic extruder machine to obtain more data and to verify or change the dynamics per need.

Throughout the course of the project, Matlab was the main tool to analyze the nonlinearity and Simulink was used to simulate the system using linearized transfer functions. However, as a basis for continued or future work, a nonlinear model of the system was setup in Simulink towards the end of the project, see Appendix B. The purpose of this was to ease the implementation of the different control strategies that were discussed earlier. Due to time limits and deadlines, control methods that compensate for the nonlinearity were not implemented. The model itself, however, was satisfactorily compared with previous results and is thus a valid starting point for future work concerning the best possible control strategy for the system.

Bibliography

A simple plastic extrusion screw (2021). URL: https://www.researchgate.net/figure/A-simple-plastic-extrusion-screw_fig8_304676485 (visited on 2021-02-16).

Automation solutions for the plastics industry (2021). URL: https://www.br-automation.com/sv/industrier/plastics/automation-solutions-for-the-plastics-industry/ (visited on 2021-02-16).

Bourne-Webb, P., T. B. Freitas, and R. da Costa Gonçalves (2016). "Thermal and mechanical aspects of the response of embedded retaining walls used as shallow geothermal heat exchangers". *Energy and Buildings*.

Convection Heat Transfer Coefficient (2021). URL: https://www.sciencedirect.com/topics/engineering/convection-heat-transfer-coefficient (visited on 2021-02-24).

Convective Heat Transfer Coefficients Table (2021). URL: https://www.engineersedge.com/heat_transfer/convective_heat_transfer_coefficients__13378.htm (visited on 2021-02-24).

Department of Automatic Control, L. T. H. (2021). *Reglerteknik - formelsamling*. URL: https://www.control.lth.se/fileadmin/control/Education/EngineeringProgram/FRTF05/formelsamling.pdf (visited on 2021-03-17).

Fan Performance and Fan Laws (2021). URL: https://fluidflowinfo.com/fan-performance-and-fan-laws/ (visited on 2021-03-12).

Fundamentals of lambda tuning (2021). URL: https://www.controleng.com/articles/fundamentals-of-lambda-tuning/ (visited on 2021-05-28).

Global production of plastics since 1950 (2021). URL: https://www.statista.com/statistics/282732/global-production-of-plastics-since-1950/#:~:text=In%202019%2C%20the%20global%20production,quarter%20of%20the%20global%20production (visited on 2021-02-16).

Joseph Black (1728-1799): Discoveries (2021). URL: https://digital.nls.uk/scientists/biographies/joseph-black/discoveries.html (visited on 2021-02-16).

Pump Theory - Euler's Turbomachine Equations (2021). URL: https://www.nuclear-power.net/nuclear-engineering/fluid-dynamics/centrifugal-pumps/eulers-turbomachine-equations/ (visited on 2021-02-22).

Tipler, P. and G. Mosca (2007). *Physics - For scientists and engineers*. 6th edition. W.H. Freeman & Co.

A

Data Sheet of the Centrifugal Fan

This appendix presents the data sheet of the centrifugal fan that was modelled in the thesis project.

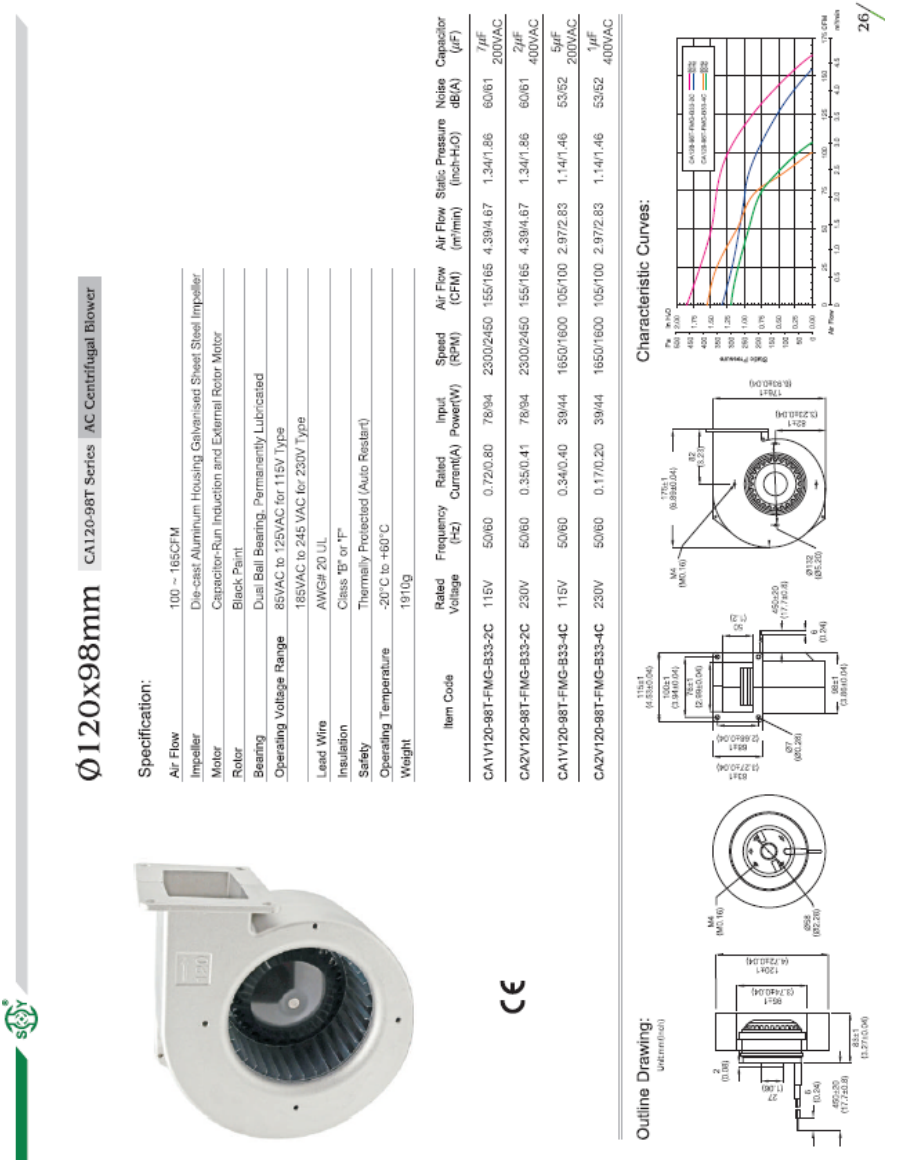

Ø120x98mm CA120-98T Series AC Centrifugal Blower

Specification:

Air Flow	100 ~ 165CFM
Impeller	Die-cast Aluminum Housing Galvanised Sheet Steel Impeller
Motor	Capacitor-Run Induction and External Rotor Motor
Rotor	Black Paint
Bearing	Dual Ball Bearing, Permanently Lubricated
Operating Voltage Range	85VAC to 125VAC for 115V Type
	185VAC to 245 VAC for 230V Type
Lead Wire	AWG# 20 UL
Insulation	Class "B" or "F"
Safety	Thermally Protected (Auto Restart)
Operating Temperature	-20°C to +60°C
Weight	1910g

Item Code	Rated Voltage	Frequency (Hz)	Rated Current(A)	Input Power(W)	Speed (RPM)	Air Flow (CFM)	Air Flow (m³/min)	Static Pressure (inch-H₂O)	Noise dB(A)	Capacitor (μF)
CA1V120-98T-FMG-B33-2C	115V	50/60	0.72/0.80	78/94	2300/2450	155/165	4.39/4.67	1.34/1.86	60/61	7μF 200VAC
CA2V120-98T-FMG-B33-2C	230V	50/60	0.35/0.41	78/94	2300/2450	155/165	4.39/4.67	1.34/1.86	60/61	2μF 400VAC
CA1V120-98T-FMG-B33-4C	115V	50/60	0.34/0.40	39/44	1650/1600	105/100	2.97/2.83	1.14/1.46	53/52	5μF 200VAC
CA2V120-98T-FMG-B33-4C	230V	50/60	0.17/0.20	39/44	1650/1600	105/100	2.97/2.83	1.14/1.46	53/52	1μF 400VAC

Outline Drawing:

Characteristic Curves:

26

Figure A.1: Data sheet of centrifugal fan.

B

Simulink Model for Future Work

The Simulink model that contains the nonlinear dynamics is presented briefly in this appendix chapter. The dynamics from Equation 3.6 are presented in Simulink blocks such as *integrators*, *gains*, *constants* and *scopes*, see Figure 5.6. The dynamics are then encapsulated in a *subsystem* and incorporated into a control loop, see Figure B.2. A suggestion for future work is to use this model with the control loop to investigate and implement different linear or nonlinear controllers.

To verify and validate this nonlinear Simulink model, simple step responses and setpoint changes were run, see Figure B.3 and Figure B.4 respectively. After a comparison with previous results, this nonlinear Simulink model is ascertained as valid.

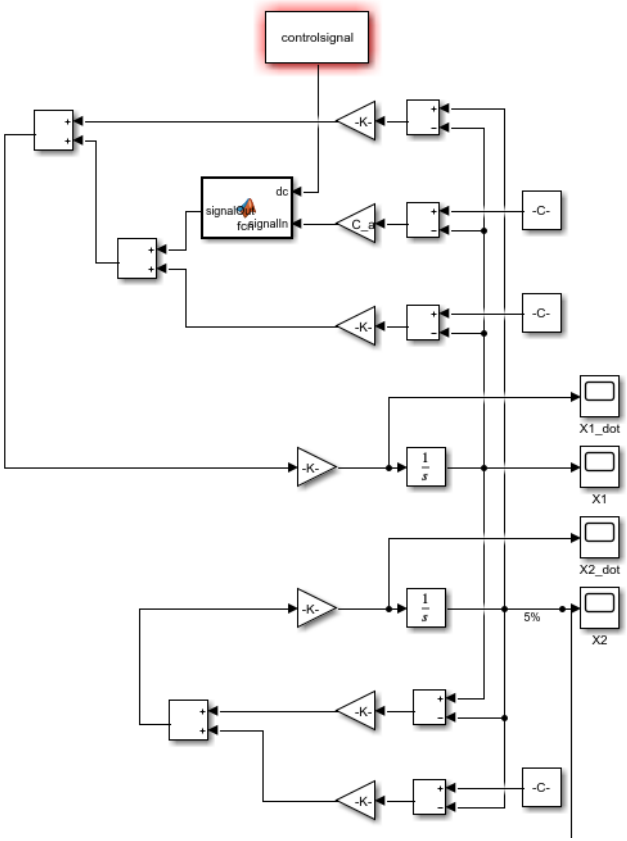

Figure B.1: Simulink nonlinear model, using airflow approximation seen in Figure 5.6.

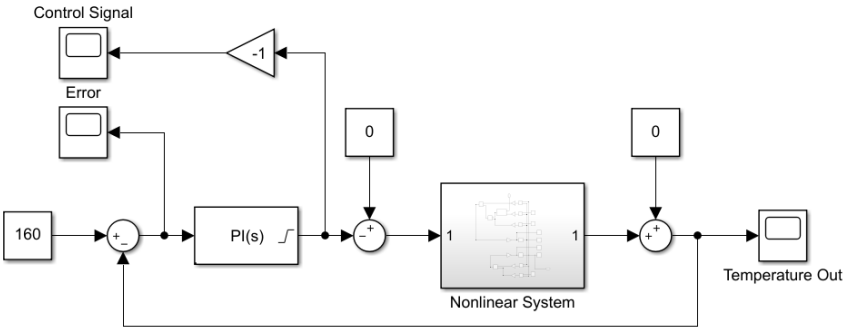

Figure B.2: PI controller for the nonlinear system.

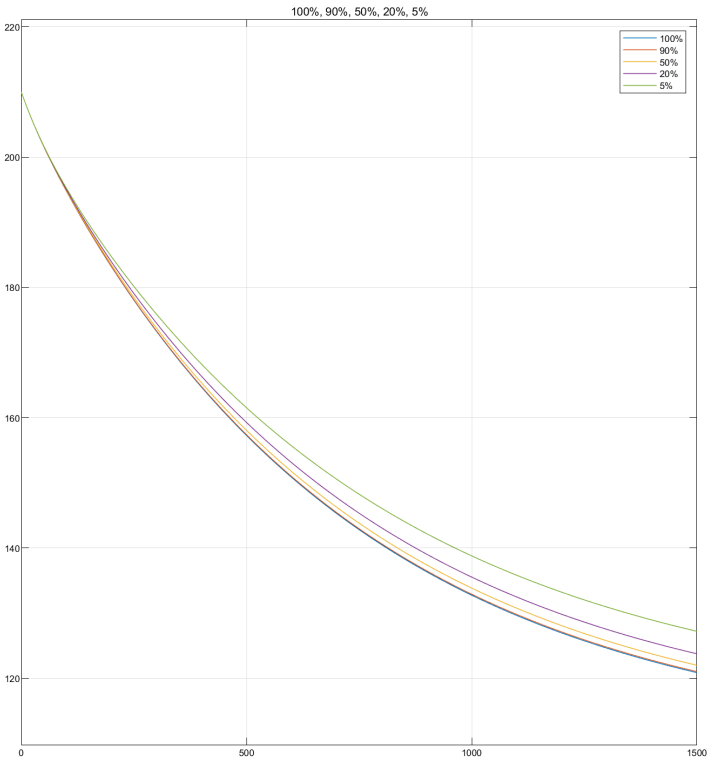

Figure B.3: Simulink nonlinear step response.

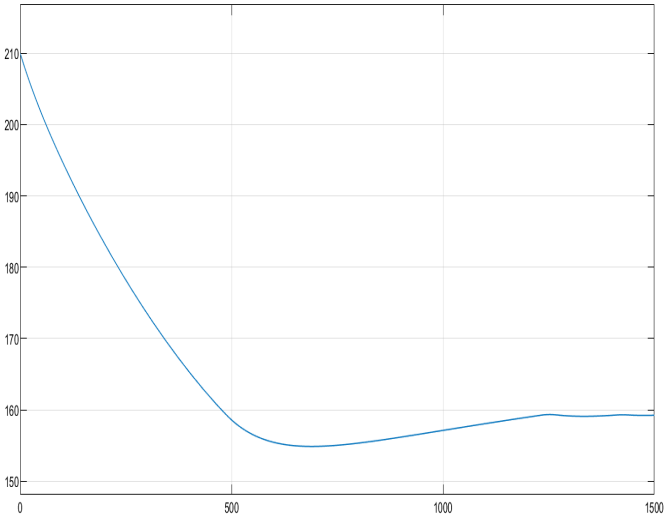

(a) System response.

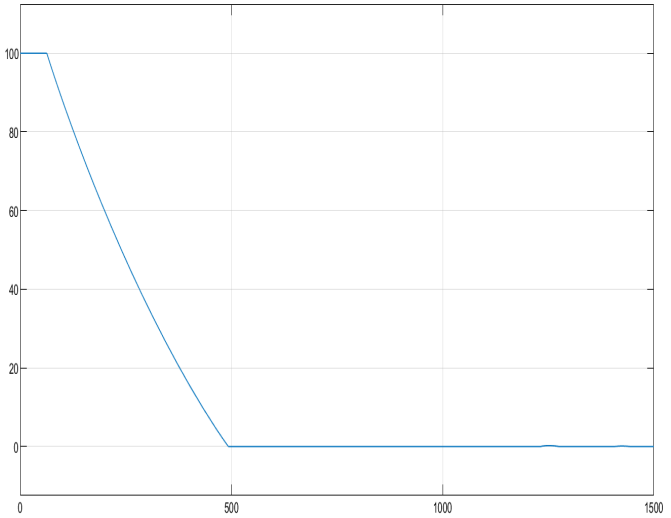

(b) Control signal.

Figure B.4: System responding to a setpoint change using a PI controller.

Lund University
Department of Automatic Control
Box 118
SE-221 00 Lund Sweden

Document name
MASTER'S THESIS

Date of issue
June 2021

Document Number
TFRT-6132

Author(s)
Christopher Fritzon
Nils Persson

Supervisor
Erik Ottosson, B&R Industrial Automation AB, Sweden
Martin Staudecker, B&R Automation Austria
Tore Hägglund, Dept. of Automatic Control, Lund University, Sweden
Anders Robertsson, Dept. of Automatic Control, Lund University, Sweden (examiner)

Title and subtitle
Modelling and Control of an Extruder Cooling System

Abstract

The thesis aims to develop knowledge of the physics and thermodynamics behind a nonlinearity in an air cooling system for an plastic extruder machine. To accomplish this, both nonlinear and linearized models were set up in Matlab and Simulink environments based on the laws of physics and thermodynamics. Simulations were run to achieve and analyze step responses, and different PI control structures were simulated and discussed. The dynamics of the centrifugal fan were pointed out as the primary reasons for the nonlinearity. Finally, different options and alternatives, both mechanical and software based, to compensate for the nonlinearity were presented.

Due to Covid-19, it was not possible to perform any tests on real hardware which was highly desirable. Instead, the results obtained in this thesis are base solely on theoretical discussions and simulations. Aspects that potentially could have been discovered through mechanical tests are therefore not considered.

Keywords

Classification system and/or index terms (if any)

Supplementary bibliographical information

ISSN and key title
0280-5316

ISBN

Language
English

Number of pages
1-78

Recipient's notes

Security classification